COMPUTATIONAL AND STRUCTURAL BIOTECHNOLOGY JOURNAL

Review

The bioenergetics of integrin-based adhesion, from single molecule dynamics to stability of macromolecular complexes

Laurent MacKay [a], Anmar Khadra [a,*]

[a] Department of Physiology, McGill University, 3655 Promenade Sir William Osler, Montreal, Quebec, Canada

ABSTRACT

The forces actively generated by motile cells must be transmitted to their environment in a spatiotemporally regulated manner, in order to produce directional cellular motion. This task is accomplished through integrin-based adhesions, large macromolecular complexes that link the actin-cytoskelton inside the cell to its external environment. Despite their relatively large size, adhesions exhibit rapid dynamics, switching between assembly and disassembly in response to chemical and mechanical cues exerted by cytoplasmic biochemical signals, and intracellular/extracellular forces, respectively. While in material science, force typically disrupts adhesive contact, in this biological system, force has a more nuanced effect, capable of causing assembly or disassembly. This initially puzzled experimentalists and theorists alike, but investigation into the mechanisms regulating adhesion dynamics have progressively elucidated the origin of these phenomena. This review provides an overview of recent studies focused on the theoretical understanding of adhesion assembly and disassembly as well as the experimental studies that motivated them. We first concentrate on the kinetics of integrin receptors, which exhibit a complex response to force, and then investigate how this response manifests itself in macromolecular adhesion complexes. We then turn our attention to studies of adhesion plaque dynamics that link integrins to the actin-cytoskeleton, and explain how force can influence the assembly/disassembly of these macromolecular structure. Subsequently, we analyze the effect of force on integrins populations across lengthscales larger than single adhesions. Finally, we cover some theoretical studies that have considered both integrins and the adhesion plaque and discuss some potential future avenues of research.

© 2020 The Authors. Published by Elsevier B.V. on behalf of Research Network of Computational and Structural Biotechnology. This is an open access article under the CC BY-NC-ND license (http://creativecommons.org/licenses/by-nc-nd/4.0/).

Contents

* Corresponding author.
  E-mail addresses: laurent.mackay@mail.mcgill.ca (L. MacKay), anmar.khadra@mcgill.ca (A. Khadra).

1. Introduction

The joint effect of the chemical and mechanical environment a cell experiences influences it behaviour across many timescales. For example, on short timescales (minutes to hours) a cell may exhibit motile behaviour in response to chemical and mechanical cues [1,2], while on longer timescales (hours to days) these same cues affect cell survival and differentiation into distinct lineages [3–6]. Although associated with behaviour at comparatively short timescales, cellular motility plays a central role in a number of long-lasting physiological and pathophysiological processes [7–9]. The visualization of its associated displacements of molecules [10–16], cellular structures [17–20], and cells [21–24] have made it an alluring area of research across many fields. Fluorescence-based microscopy has not only allowed for the visualization of these displacements, but also the biochemical characterization of the structures involved. In conjunction with biochemical and genetic manipulations, fluorescence-based microscopy data has resulted in an extensive literature detailing the processes involved in motility across many lengthscales: from the single molecule scale to the tissue-level scale. A significant challenge in the field has been to take these complex, and sometimes seemingly contradictory, experimental characterizations and arrive at a mechanistic understanding of what drives a specific cellular behaviour. While proper experimental design is crucial in this endeavour, theoretical models, both mathematical and computational, have proven to be useful in providing a level of control, spatiotemporal resolution, visualization, and quantification that may go well beyond what can be achieved experimentally.

The motile behaviour of cells highlights the importance of force-generation in cells, which is largely thought to arise from a combination of actin polymerization and myosin-driven contraction [25]. However, in order for directed cellular motion to occur, the internal forces of the cell must be transmitted to its environment. One means by which cells accomplish this force transmission are integrin-based adhesions, macromolecular structures that act as a mechanical linkage between the cell's environment and its actin-cytoskeleton [25,26]. Interestingly, integrin-based adhesions are mechanosensitive, assembling and adjusting their size and strength in response to force [18,17,27–32]. The highly dynamic nature of these relatively large structures poses a significant modeling challenge as it involves interactions across many length- and timescales. Indeed, adhesions are formed as the result of interactions between over 100 different proteins which often exhibit some form of redundancy [33], making it difficult to both isolate key players and determine how nuanced interactions may lead to divergent behaviours. Nonetheless, many models of adhesions and the molecules which comprise them have been successful in furthering our understanding of adhesion dynamics and the role that forces play in determining these dynamics.

In this review we will cover some of these models and the experimental findings which motivated their formulation. In particular, we will focus on the mathematical forms which give rise to specific model behaviours, and the relation these forms have to the underlying physics and biological structure of adhesions. The emphasis on mathematical forms is made to help clarify the critical determinants of cellular behaviour rather than the specific results of a simulation which may depend heavily on indeterminate parameter values. We will see how these mathematical forms are used to predict both steady-state and transient behaviours of this system at the single-molecule, adhesion, and membrane level.

This review is organized as follows. First, we briefly discuss the architecture of adhesions and how it relates to their function, and then highlight some aspects of the adhesion life cycle which will be relevant to modeling. The bulk of the review will then be allocated to covering various mathematical models which have yielded insight into the dynamics of adhesions. Broadly speaking, we will focus on models have that either analyzed integrins receptors and their bonds to ligands or studied the condensed phase of adaptor proteins which form a plaque that sits atop the integrins. First, we will show how a combination of experiments and modeling have enriched our understanding of single integrin dynamics, and then explore how the properties of the integrin-ligand bond can be incorporated into bond-cluster models that predict the mechanical response of a collection of integrin receptors. Subsequently, we will cover some theoretical treatments of the adaptor protein plaque and its response to anisotropic applied forces. This will be followed by briefly describing a model that helped bridge the two classes of models of adhesions, and reconcile some of the differences between the outcomes of the two classes of models. Finally, we will draw some conclusions and give an outlook on future challenges in the field. An appendix detailing the common thermodynamic formulation of the models presented here is also included at the end of the review.

2. Biological background

2.1. Adhesion architecture

Adhesions are comprised of a very large number of dynamically interacting proteins to produce a bio-mechanically regulated force transmission point between a cell's actin-cytoskeleton and its environment [33]. Central to this force transmission is the integrin receptor, a heterodimeric transmembrane protein which binds extracellularly to ligands typically found in connective tissue and whose cytoplasmic domain is linked to the actin-cytoskeleton through interactions with adaptor proteins (see Fig. 1, [34,26]). Adaptor proteins are a class of cytosolic proteins which form a membrane-proximal plaque. This plaque aides in the spatial
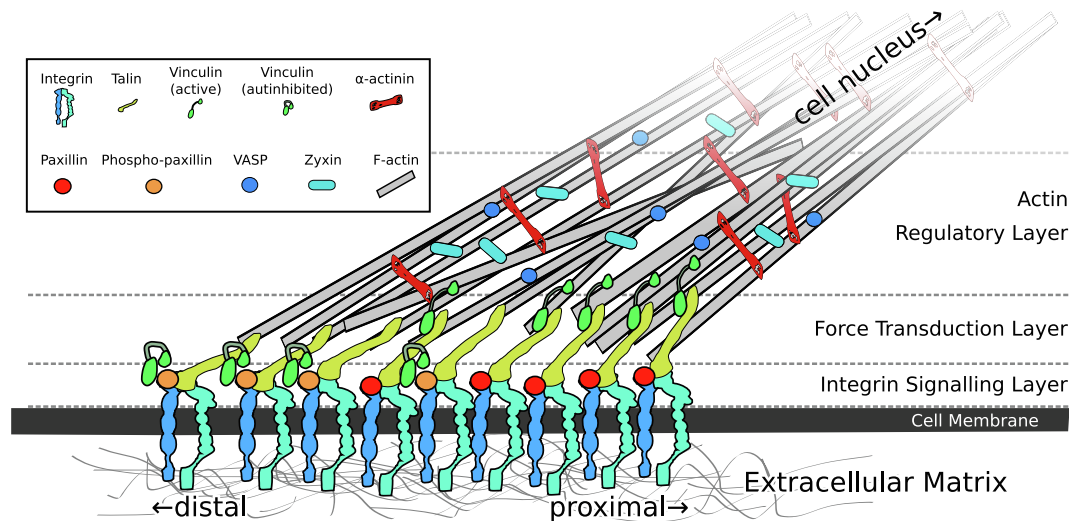
Fig. 1. Structural diagram of the nanoscale architecture of integrin-based adhesions in a protrusive region of a motile cell. Integrin receptors span the cell membrane, binding to ligands in the extracellular matrix. Their cytoplasmic tails are complexed with adaptor proteins, forming an adhesion plaque that connects them to F-actin. The integrin signaling layer is the juxtamembrane region (10–20 nm in thickness) where adaptor proteins involved in signaling pathways are found (e.g., paxillin). Above this layer is the force transduction layer (terminating cytosolically 50–60 nm above the membrane) enriched with talin and active vinculin, proteins that form a linkage between the actin-cytoskeleton and integrin. Finally, the actin regulatory layer contains proteins that help organize actin into contractile stress fibres. A stress fibre typically points from the adhesion towards the cell nucleus; this directionality is used to define the adhesion's frame of reference in which distal (proximal) refers to the tip furthest away from (closest to) the nucleus. A gradient in paxillin phosphorylation leads to an asymmetry in the distribution of active vinculin [49,15], while the elastic response of the adhesion plaque has been theorized to produce a gradient in the tilt of proteins in the transduction layer [40]. Figure adapted from [26] and [40].

organization of integrins, into discrete adhesions [35,36,16], and serves as a mechanical linkage between integrins and the actin-cytoskeleton. The adhesion plaque is formed as a result of adaptor proteins binding to integrins as well as one another. Aggregation of adaptor proteins leads to the growth of the adhesion plaque through adsorption, while the reverse process of desorption may explain shrinkage of the plaque [37–40,19]. The term net adsorption will be used to refer to the combined effect of both processes. Biochemical signaling events and mechanical forces have both been implicated in modifying the propensities of these adsorption/desorption processes, providing the cell with means to dynamically alter the size and stability of adhesions.

The adhesion plaque is divided into functionally distinct layers (see Fig. 1, [41,15]). The lowest layer is known as the integrin signaling layer (terminating cytosolically 10–20 nm away from the membrane), where adpator proteins are closely associated with integrins, allowing paxillin- and FAK-dependent signals to relay information about the integrin-ECM linkage to various biochemical signaling pathways [42,43]. Above the signaling layer lies a force transduction layer (terminating cytosolically 50—60 nm away from the membrane) which links integrins to filamentous actin (F-actin), and is primarily comprised of talin (which both activates integrins and binds to F-actin [44]) and vinculin (which reinforces the talin-actin bond [45,46]); this latter layer is responsible for the transmission of forces from the actin-cytoskeleton to integrins. One would expect the many proteins in the force transduction layer to be associated with actin filaments, which requires actin filaments to be brought into contact with the adhesion. Consequently, immediately above the transduction layer, is an actin regulatory layer which contains the proteins VASP, zyxin, and α-actinin [41]. The proteins in this uppermost regulatory layer promote filament growth and F-actin bundling into very stable and contractile stress fibres [47,48]. This means that these three functional layers interact to self-assemble into the mechanical linkage between the actin-cytoskeleton and the external environment [26]. Within this framework, the signaling layer contains the mechanical link to the external environment (i.e., integrins), the transduction layer connects these integrins to the actin-cytoskeleton, and the regulatory layer helps to organize the actin-cytoskeleton around the adhesion into structures that produce the force transmitted through integrins to the external environment.

2.2. Adhesion life cycle in motile cells

Focal adhesions form through a series of biochemically- and mechanically-driven steps. They initially start as highly dynamic nanoscale clusters of integrins, termed nascent adhesions (NAs), in the lamellipodium [50], a morphological compartment with a very dense quasi-two-dimensional polymerizing actin meshwork. This semi-rigid network of F-actin projects from the actin-cytoskeleton to form the leading edge of a polarized cell [51], while the polymerization of the filaments drives the leading edge forward by using NAs as anchor points [52,53]. As the leading edge of a migrating cell moves forward, so does its lamellipodium; once a NA is no longer covered by the lamellipodium it disassembles rapidly [19]. However, a small fraction of NAs stabilize and persist beyond the lamellipodium, growing centripetally inwards into mature focal complexes (FCs) and focal adhesions (FAs) [19,54].

The decision for a NA to disassemble or initiate its maturation is regulated biochemically by changes in the molecular state of adaptor proteins (e.g., phosphorylation of FAK or paxillin) [55,49,56]. From a mechanical perspective, maturation is associated with an increase in traction stress [57,58,31]. Therefore, it is not surprising that the association of a FA with a contractile actin stress fibres results in its stabilization [30]. As the whole cell moves forward, its FAs either gradually disassemble as they steadily move towards the cell rear [59], or, in some cell types, they may become highly stable fibrillar adhesions which form as a result of cell-dependent reorganization of the ECM [60]. In fibroblasts, the former effect is fairly robust with only ~10% of FAs at the trailing edge originating from the front of the cell, whereas trailing FAs primarily originate in small protrusions at the rear and lateral zones of the cell [59].

The spatiotemporal regulation of disassembly for non-fibrillar FAs remains incompletely understood. Yet, it has been found that (i) FAs undergo repeated periods of disassembly which are

correlated with their proximity to the growing tips of microtubules [59], (ii) microtubule tips are targeted to FAs in a paxillin-dependent manner [61], and (iii) abrogating microtubule growth halts the disassembly of FAs [62,63]. Interestingly, this microtubule-dependent disassembly seems to be mediated by clathrin-dependent endocytosis of integrins [64–66], while other internalization routes (e.g., caveolin-dependent endocytosis) may also contribute to adhesion disassembly [67]. Furthermore, in some cellular contexts, internalization may be further aided by the exocytosis of matrix metalloproteases that degrade the ECM [68,69]. For more on the interplay between microtubules and adhesions or the internalization of integrins, we refer the reader to the reviews by Seetharaman and Etienne-Manneville [70], or De Franceschi et al. [67], respectively.

Within motile cells, FAs that form at the front of the cell are effectively immobile relative to the ECM. When these FAs reach the rear of the cell they must disassemble in order for the cell to continue migrating. FA-disassembly at the cell rear allows for the trailing membrane to roll forward which in turn permits further extension of the lamellipodium. While the presence of FAs in this region of the cell is necessary for proper cell spreading and resisting the tension generated in the lamellipodium, their timely disassembly is necessary for efficient cell migration. This disassembly occurs primarily by two means: integrin/adhesion release and adhesion sliding.

Integrins are "released" from the trailing edge of a migrating cell [71,72]. On a highly adhesive ECM, this process is caused by intracellular breakage of the FA plaque-integrin linkage, leaving integrins stuck to the ECM after the trailing edge moves forward; on the other hand, on less adhesive substrates, release of integrins from the cell is infrequent with breakage occurring extracellularly at the integrin-ECM linkage [72], a process we term adhesion release. Regardless of the adhesiveness of the ECM, however, strong traction forces produced by RhoA-dependent myosin-driven contraction of the actin cytoskeleton drive the breakage of bonds that hold the FA together, leading to their disassembly. At least two biochemical mechanisms have been identified as modulators of adhesion release. First, the calpain family of intracellular Ca^{2+}-dependent proteases have been shown to cleave a number of FA proteins which can (directly or indirectly) mechanically decouple integrins from the actin cytoskeleton [72–75]. Second, in lymphocytes, it has been experimentally found that the protein SHARPIN associates with the integrin (LFA-1) preferentially at the cell rear and maintains it in a low-affinity inactive conformation that facilitates the mechanical breakage of the integrin-ligand bond [76,77]. Notably, this low affinity state does not exhibit the normal mechanosensitive binding properties of the integrin bond [78,77].

Alternatively, adhesion sliding may also occur in a subset of FAs at the cell rear [79], and unlike integrin release, it is not migration-dependent [80], but is a tension-dependent process [81]. During FA-maturation, the proximal tip of an elongated adhesion grows more rapidly than the distal tip shrinks, leading to further elongation [18,19], in contrast to adhesion sliding where the distal tip typically shrinks more rapidly than the proximal tip grows. This striking phenomenon leads to an apparent sliding of FAs towards the center of the cell, and a gradual decrease in their size. Although these sliding adhesions visually appear to exhibit slippage, this phenomenon is more likely due to an asymmetry in matter exchange rates between the two tips of adhesions [81,12,82]. Biochemically, a number of proteases have been implicated in this process [82], but as we shall see in this review, a number of mechanical effects may also be implicated in adhesion sliding.

3. Integrin activation and mechanosensitivity

Integrin receptors exist as non-covalently bonded heterodimeric pairs of α and β subunits. There are 18 α and 8 β subunits in vertebrates, which allow different cell-types to exhibit diverse responses to extracellular signals through differential ECM ligand binding, cytoskeletal association, and biochemical signaling [83]. Initial crystal structures of integrins showed that the heads of the extracellular domains of both α and α subunits are bent towards the membrane [84]. This conformation is now regarded as the inactive form of the integrin receptor, capable of binding to ligands with a low affinity. In order for the receptors to bind their ligands with high affinity, integrins must first become activated through global conformational changes that expose the binding head of the receptors [85]. This conformational change can be induced chemically by replacing extracellular Ca^{2+} with Mg^{2+} or Mn^{2+}, resulting in an equivalent change in the identity of the divalent cation contained in the metal-binding sites of the integrin receptor [86,87]. Alternatively, the binding of the cytoplasmic protein talin to the intracellular tail of the β subunit has also been found to activate integrins through equivalent conformational changes [88,89]. The latter form of activation is the more physiologically relevant pathway and is termed inside-out activation, which is associated with numerous downstream signaling effects [90,91].

During the conformation changes associated with activation, integrins become extended in such a way that their binding heads points towards extracellular ligands [85]. In this extended state, the binding head can be either in a closed or an open state [92]. It was previously shown that the opening of the headpiece is the step required for high affinity binding [93]. This was in line with molecular dynamics simulations suggesting that an intermediate affinity state could correspond to a force-stabilized intermediate step in the physical extension of the α subunit that is associated with the switch from the low affinity inactive state to the high affinity active state [94,95]. Such a view agrees with the experimental observation that activated integrins typically exhibit less ligand binding than that of the high affinity binding state induced by divalent cations, with the high affinity state being achieved transiently in some activated cells [96–99]. Based on this, we can conclude that the complete integrin activation process involves the extension of the receptor followed by the opening of the headpiece, and that the extended state with a closed headpiece may represent a force-induced partially activated state. The three major *active* and *inactive* conformations of integrin can thus be described as follows:

1. The *inactive* bent closed (BC) conformation that has its binding head bent towards the membrane, away from extracellular ligands, and binds ligand with a low affinity.
2. The *inactive* extended closed (EC) conformation that has its legs extended, with the binding head pointing away from the membrane (towards extracellular ligands), and exhibits a low binding affinity due to a partially occluded binding site.
3. The *active* extended open (EO) conformation that has its legs not only extended but also separated, reflecting the opening of the headpiece, and as a result exhibits high binding affinity.

While the structural details of the activation process have been studied extensively, some questions still remain. In particular, what are the relative contributions of mechanical and chemical cues in the activation process? Can either effect explain activation alone? How do these aforementioned conformational changes manifest themselves in the ligand binding kinetics of integrin?.

3.1. Mechanism of activation

Differences in the structural and functional properties of the three conformations, mentioned above, have lead to the genesis of the so-called force-activation hypothesis [83]. Within this framework, it is assumed that naive receptors are overwhelmingly found in the BC conformation, but upon loading them with mechanical force, the extended conformations (EC & EO) of integrin are stabilized by the work needed to refold the protein under load [94,95,100]. This allows integrins to be primed for higher affinity ligand binding through the application of force [101,102]. Because integrins are the primary component of adhesions, their mechanosensitive affinity regulation has been posited as a possible mechanism for the initiation of cellular responses to force [20].

We now ask whether or not force activation is the unique mechanism of activation. As mentioned above, binding of talin (or kindlin, [103]) to integrins cytoplasmic tails is widely regarded as the biochemical step necessary for activation. However, it is unclear if talin binding is sufficient for activation. In other words, can a lack of mechanical activation be compensated for by a high enough talin concentration? A recent theoretical study by Li and Springer has investigated this question using a thermodynamic approach to model the conformational equilibria of $\alpha_5\beta_1$ integrin receptors [104]. To quantify the probability of activation as both the force and the concentration of relevant chemical species (e.g., talin and fibronectin) are varied, they considered the molar free energy of the bare receptors (i.e., their reference chemical potential μ^0 as determined by fluorescence polarization [100], see Appendix A for more on μ^0). They also included the contributions of relevant chemical reactions as well as the mechanical work needed to revert a receptor back to its inactive BC conformation. In particular, they assumed that integrins are only loaded with force when bound to both a cytoplasmic adaptor protein and an extracellular ligand, In this case, an integrin receptor has a chemical potential given by

$$\Delta\mu_i = \mu_i^0 - k_B T \ln\left(C_{\mathrm{ada}}/K_{\mathrm{ada}}^i\right) - k_B T \ln\left(C_{\mathrm{lig}}/K_{\mathrm{lig}}^i\right) - F\Delta x^i, \tag{1}$$

where $i \in \{\mathrm{BC}, \mathrm{EC}, \mathrm{EO}\}, C_{\mathrm{ada}}$ (C_{lig}) is the concentration of adaptor proteins (extracellular ligands), K_{ada}^i (K_{lig}^i) is the experimentally determined dissociation constant for complexes formed between an integrin with conformation i and adaptor proteins (extracellular ligand), F magnitude of the applied force, and Δx^i is the characteristic displacement length of conformation i relative to the BC conformation (i.e., $\Delta x^{\mathrm{BC}} = 0$). We note here that the original study used the symbol ΔG_i rather than $\Delta\mu_i$ to denote the molar Gibbs free energy, however since the systems under consideration are individual molecules these two quantities are equivalent (see Appendix A.1). The probability of being in an active state in the absence of applied force was then computed using the Boltzmann distribution, where in the absence of applied force, $\sim 99.7\%$ of $\alpha_5\beta_1$ integrins were expected to be in the inactive BC conformation. In comparison, the conformational equilibria of $\alpha_4\beta_1$ integrins were found to have $\sim 98.4\%$ of integrins in the BC conformation (i.e., $\sim 1.0\%$ of $\alpha_4\beta_1$ are in the active EO conformation compared to $\sim 0.17\%$ for $\alpha_5\beta_1$), suggesting that the conformational energies of $\alpha_4\beta_1$ integrins may prime them for the rapid adhesion involved in rolling leukocyte extravasation [105,106].

While Eq. (1) is only part of the complete thermodynamic model, it highlights the dependence of free energy on chemical and mechanical contributions. Changes in chemical concentration affect free energy in a logarithmic manner, while changes in mechanical force have a linear effect on the free energy. Thus under the physiological assumption that both ligand and adaptor proteins are present at non-zero concentrations, variations in their concentration will have little effect on the outcome of the activation process. On the other hand, mechanical force has a much more potent effect, with an intrinsic free energy difference between the BC and EO conformation ($\mu_{\mathrm{EO}}^0 - \mu_{\mathrm{BC}}^0$) equivalent to only ~ 1 pN of applied force when $\Delta x = 14.5$ nm [104]. This suggests that integrin activation is ultra-sensitive to changes in applied force, with an activation probability that can jump from ~ 0 to ~ 1 over a range of only ~ 2 pN. We note here that this force range should be readily attained in networks of polymerizing F-actin (~ 1 pN per filament, [107,108]). Chemical effects, on the other hand, produce a much more graded response, requiring chemical concentrations to vary over many orders of magnitude to produce significant changes in extension/activation of integrin receptors. Due to the rapid dynamics of integrin activation [109], the extension of integrins, and their subsequent activation, seems much more likely to be caused by mechanical forces than by chemical effects. It is important to point out here that, at very low adaptor protein concentrations, the second term in Eq. (1) will dominate over μ_i^0, indicating that almost no receptors will be bound to an adaptor protein due to the chemical potential of adaptor-bound conformations being exceedingly high. In such a scenario, the force-dependence of activation will vanish, as almost no receptors will be loaded with force. This implies that, neither talin binding nor mechanical forces are sufficient for activation, rather both are necessary. Interestingly with a physiologically reasonable applied force of 1.5 pN [110], the energy differences intrinsic to $\alpha_4\beta_1$ also seems to give these integrins enhanced sensitivity to changes in adaptor protein concentration/affinity relative to $\alpha_5\beta_1$ [105]. Furthermore, the intrinsic conformational energies were also found to vary across cell-types [105]. These cell-specific differences were likely due to variations in physicochemical environments, which may be caused by differences in membrane composition and cytoplasmic proteins that interact with integrins such as adaptor proteins or inhibitors of activation [105]. This variability highlights that the interplay between chemical and mechanical effects is non-trivial as well as cell- and integrin subtype-specific, but that it may be explored using the thermodynamic framework developed by Li and Springer. For more on the mechanosensitive activation of integrins, we refer the reader to the reviews by Sun, Costell, and Fassler [111] as well as Kechagia, Ivaska, and Roca-Cusachs [112].

3.2. Unbinding kinetics of integrin

While we have seen how structural changes in integrin receptors can lead to their activation and how these changes are driven by a combination of mechanical and chemical effects, it remains unclear how such processes manifest themselves in the dynamics of adhesions. To answer this question, we will first explore how the conformational changes discussed above result in a very specific mechanical response for integrin receptors using a combination of theoretical and experimental perspectives. In order to appreciate the richness of the resulting behaviour, we begin by considering a generic theory for the unbinding of molecular bonds under mechanical load. In [113], a phenomenological expression for the rate of unbinding of a collection of molecular bonds all experiencing a mechanical load F was originally proposed by Bell; it was given by $k_{\mathrm{off}} \propto \exp\left(F/F_0\right)$. Such an expression may be derived from Eq. (A.11) by accounting for the work done by the force $\vec{F}\left(\vec{\ell}\right)$ along the reaction path $\vec{\ell}$ starting from the bound state; that is

$$\mu(x) = \mu^0(x) + \int_x^{x_0} \vec{F}\left(\vec{\ell}\right) \cdot d\vec{\ell}, \tag{2}$$
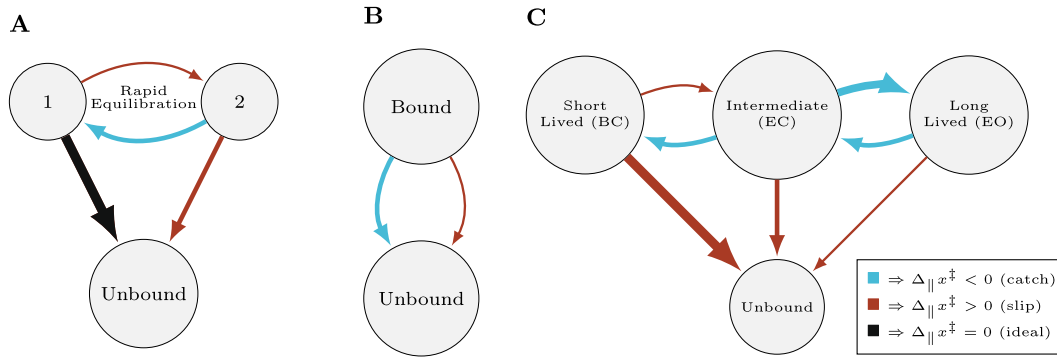
$$= \mu^0(x) + \mu_F(x)$$

Fig. 2. Models of integrin unbinding kinetics. (A & B) Two generic models of catch bonds: the two bound state model [117] (A), and the two-pathway model [119] (B). (C) Kinetic model of the mechanosensitive integrin-ligand bond that explains cyclic mechanical reinforcement [102]. Arrow thickness reflects the transition rate between the different states in the absence of force: the thicker the arrow, the the faster rate in the absence of force. In all three models, as force is varied, the transition rates of the transitions depicted by red (blue) arrows increase (decrease), resulting in the observed catch bond behaviour. The black arrow in A signifies an ideal bond whose unbinding rate does not vary with force. (For interpretation of the references to colour in this figure legend, the reader is referred to the web version of this article.)

where x is the position of bonded molecule, x_0 is the position of the bound state, $\mu^0(x)$ is its chemical potential in the absence of force, $d\vec{\ell}$ is the infinitesimal displacement of the molecule along the reaction path from the bound state, and $\mu_F(x)$ is the chemical potential due to the applied force. Using Eq. (A.11), we may arrive at $k_{off} \propto \exp\left(-\Delta\mu_0^{\ddagger}/k_BT\right)\exp\left(\int_{x^{\ddagger}}^{x_0}\vec{F}\left(\vec{\ell}\right)\cdot d\vec{\ell}/k_BT\right)$, where $x^{\ddagger}$ is the position of the transition state and $\Delta\mu_{\ddagger}^0 = \mu^0(x^{\ddagger}) - \mu^0(x_0)$ is the intrinsic chemical potential difference of the transition state in the absence of force. It is indeed possible to use spatial potentials to investigate the unbinding rate in a way that actually considers the reaction path, revealing a threshold in force ramping rate required to produce a force-dependent unbinding rate [114]. Moreover, such predictions have lead to an experimentally validated theory of dynamic force spectroscopy for weak non-covalent bonds [115]. However, it is more common to simply abstract the molecular movements and rewrite the integral as $\Delta\mu_{\ddagger} = \Delta\mu_{\ddagger}^0 - F\Delta_{\parallel}x^{\ddagger}$ where $\Delta_{\parallel}x^{\ddagger}$ is the displacement from the bound state to the transition state parallel to the direction of the force. Defining the bound state as having a chemical potential of zero, we may use Eq. (A.11) to compute the unbinding rate as

$$
\begin{aligned}
k_{off}(F) &= \gamma\exp\left(-\Delta\mu_{\ddagger}/k_BT\right) \\
&= \gamma\exp\left(-\Delta\mu_{\ddagger}^0/k_BT\right)\exp\left(F\Delta_{\parallel}x^{\ddagger}/k_BT\right) \\
&\propto \exp\left(F/F_0\right),
\end{aligned}
\tag{3}
$$

where $\gamma > 0$ is a kinetic parameter and $F_0 = k_BT/\Delta_{\parallel}x^{\ddagger}$ is a force scale that characterizes the force-dependence of the transition. Here, we have assumed that the position of the transition state is independent of F, which may not be strictly true, but is a common assumption in the field that agrees well with experimental measurements [114,116–119]. Such a formalism defines the behaviour of what is commonly referred to as a slip bond, where the unbinding rate increases monotonically with applied force [120,121].

Alternatively, by imposing some theoretical assumptions on the potential energy landscape of bonds involved in peeling a membrane off a surface, Dembo et al. predicted a different type of bond, a catch bond, whose off-rate decreases rather than increases with applied force [120]. They also hypothesized that such a bond may be central to a number of biological adhesion phenomenon. Initial experiments using atomic force microscopy under force-ramp conditions suggested that integrin-ligand pairs behave as slip bonds [122–124]. However, under force-clamped conditions, Kong

et al. 2009 demonstrated that these pairs can exhibit a catch bond behaviour, with a short-lived lifetime of ~ 1 s in the absence of force and a long-lived lifetime of > 10 s for forces in the 20–30 pN range [125].

A number of physically realistic yet mathematically tractable models have been proposed to explain the catch bond behaviour in a way that is more realistic than its original conception, which predicted a vanishing unbinding rate for arbitrarily large forces. Firstly, Evans et al. developed a five-parameter "state" model with two bound states (see Fig. 2A) [117]. The interconversion between the two states in this model was assumed to equilibrate rapidly, i.e.,

$$
\frac{P_1(t)}{P_2(t)} \approx \exp\left(\Delta\mu_{12}/k_BT\right) = \exp\left(\Delta\mu_{12}^0/k_BT\right)\exp\left(-F/F_{12}\right),
\tag{4}
$$

where $P_1(t)$ $(P_2(t))$ is the probability of being in the bound state 1 (2), $\Delta\mu_{12}^0$ is the intrinsic energy difference between the two bound states (in the absence of force), and F_{12} is a force-scale which characterizes the transition between states 1 and 2. Furthermore, they assumed that only bound state 2 exhibits a force-accelerated unbinding rate (i.e., $\Delta_{\parallel}x_{\ddagger,1}^{\ddagger} = 0$ and $\Delta_{\parallel}x_{\ddagger,2}^{\ddagger} > 0$) [117]. With $\Delta\mu_{12}^0 > 0$, unbinding from state 1, according to this model, dominates at low forces, while the interconversion to state 2 becomes more favourable as force is increased. Therefore, if the intrinsic unbinding rate for state 2 (k_2^0) is significantly lower than that for state 1 (k_1^0) the observed bond lifetime will increase within a force range that (i) favours the interconversion to state 2 and (ii) also satisfies the inequality $k_2^0\exp\left(F/F_2\right) < k_1^0$, producing the catch bond behaviour. Alternatively, in [119], Pereverzev et al. also developed a "pathway" model with two dissociation pathways from one bound state (see Fig. 2B). The transition states associated with each pathway are assumed to be in opposite directions when projected onto the force vector, i.e.,

$$
\Delta_{\parallel}x_c^{\ddagger} < 0 < \Delta_{\parallel}x_s^{\ddagger}
$$

where $\Delta_{\parallel}x_c^{\ddagger}$ $(\Delta_{\parallel}x_s^{\ddagger})$ is the displacement parallel to the force in the catch (slip) pathway. With this difference in sign, the force-dependent unbinding rate can be expressed as

$$
k_{off} = k_s^0\exp\left(F/F_s\right) + k_c^0\exp\left(-F/F_c\right)
\tag{5}
$$

where $F_s, F_c > 0$, and an efficient catch bond can be produced when $k_c^0 \gg k_s^0$ [119]. The state model is more consistent with the experimental evidence for multiple conformations of integrin, but it is also tempting to use the pathway model as it performs almost identically to the state model but has one less parameter to be

determined from data [119]. Interestingly, the pathway model may be derived by applying the assumption defined by Eq. (4) to a more general model of unbinding in the presence of allostery which, unlike the state model, explicitly tracks the allosteric interconversion between bound states [126,127]. This may explain the relative popularity of the two-pathway model despite the lack of evidence for multiple dissociation pathways from a single bound state [128–132]. For more on models and experiments related to bond dynamics in the context of cellular adhesion, we refer the reader to a review by Rakshit and Sivasankar [133].

Thus far we have hinted at a relation between bound states of integrins and the conformations that are associated with its activation. Interestingly, it was found that by applying cyclic forces to integrin, rather than using a constant force-clamp, the long lived bound state could be attained at significantly lower force magnitudes, an effect termed cyclic mechanical reinforcement [101]. In order to capture the history-dependence of unbinding, it was crucial to use a kinetic model with three bound states (see Fig. 2C) that unbinds according to Eq. (3) (i.e., three slip bonds) and assume that the interconversion between states is force-dependent but not instantaneous [102]. The biophysical properties of these three bound states and the sign of the force-dependence of their interconversion unambiguously allowed for ascribing an equivalence between the three bound states and the three main integrin conformations: BC, EC, and EO. This suggests that the integrin activation process is reflected in the kinetics of integrin unbinding, with each conformation behaving as a slip bond with different properties, while mechanical forces govern the interconversion between the conformations (e.g., extension is favoured in the presence of appropriately directed force) in order to produce the observed catch bond behaviour.

It is worth noting that thermodynamic model of Section 3.1 (see Eq. (1)) predicts that integrin activation can be induced by as little as ~ 2 pN of force, whereas experimental evidence suggests that the catch bond behaviour of integrins is triggered at a threshold of $\sim 10 - 20$ pN for constant forces [125,134–136], and ~ 5 pN for repetitive forces [101,102]. This discrepancy remains incompletely understood, but may be due to assumption that K_{lig}^{i} is independent of force. As we have seen in this section, integrin unbinding rates vary with force, and thus we may expect the binding affinity ($1/K_{\text{lig}}^{i}$) to vary as well. In the following section, we will show how a combination of simulations and theoretical work has been used to investigate the dependence of binding affinity on applied force in the context of generic receptor-ligand binding.

4. Normal forces and the binding affinity of transmembrane receptors

As discussed above, how applied force affects the unbinding process is now relatively well understood from a microscopic point of view. As can be seen in Eq. (2), the interaction potential $\mu^0(x)$ between the receptor and ligand pair interacts with the work done by the applied force $\Delta\mu_F(x)$. Of particular interest is the work done at the transition state $\Delta\mu_F(x^{\ddagger})$, which either aids ($\Delta\mu_F(x^{\ddagger}) > 0$) or hinders ($\Delta\mu_F(x^{\ddagger}) < 0$) the stochastic evolution of the system from the bound state to the transition state. On the other hand, during the binding process, the interaction potential is quite shallow, implying that the unbound molecules will be relatively unconstrained. This makes it unclear as to how to define x_0 in Eq. (2) for the binding process. Furthermore, prior to binding, it is somewhat ambiguous how force will modify the energy of the system given that the force applied to the receptor cannot be transmitted to the ligand and vice versa. One can intuit that the molecules under force will be displaced, such that the four factors: (i) the geometry of the molecules (i.e., not simple point particles), (ii)

the location of their binding sites (e.g., near the tip of the binding head of integrin receptors), (iii) the geometric constraints on the molecules (e.g., a trans-membrane receptor being anchored to the membrane), and (iv) the direction of the applied force, will all play important roles in determining the binding rates. Due to these displacements, it seems therefore likely that a single molecule description will not be sufficient to study the problem accurately.

To tackle this problem, recent studies [137,138] [138] have modeled the force-dependent binding affinity of generic receptor-ligand pairs as simple rods anchored to one of two apposing membranes, where the rods have binding sites at their tips. Using Monte Carlo simulations, they produced molecular dynamics (MD) data for the receptor and ligand rods diffusing along thermally fluctuating membranes as well as rotating about their respective anchor points on the membrane. This MD data was used to obtain estimates of binding affinity which were subsequently compared to results obtained from a statistical thermodynamics model (derived in these studies to describe the MD simulations) showing that they were in close agreement. While the statistical thermodynamic model used a more general framework than the one presented in Appendix A, it nevertheless did employ very similar energetic considerations. In order to understand this model, we begin first by considering the change in Gibbs free energy due to the binding of receptor-ligand pairs in free solution, given by

$$\Delta G_{3D} \approx U_0 - \underbrace{k_B T \ln\left(V_b/V\right)}_{\Delta G_{\text{trans}}} - \underbrace{k_B T \ln\left(\Omega_b/4\pi\right)}_{\Delta G_{\text{rot}}},$$

where V_b and Ω_b are the translational and rotational phase-space volumes of the bound receptor-ligand pair, V is the volume of the simulations, and U_0 is minimum binding energy [137,138]. The phase space volumes in this model were primarily determined using MD data. More specifically, it was assumed that $V_b = (2\pi)^{3/2} \xi_x \xi_y \xi_z$ where ξ_x, ξ_y, and ξ_z are the standard deviations of the distributions for the $x, y,$ and z coordinates of the binding vector that connects the two binding sites, respectively. The binding affinity was then computed using $K_{3D} = V \exp\left(-\Delta G_{3D}/k_B T\right)$, where V is the volume of the simulation. For membrane bound receptors, the separation between the two membranes, l, is critical in determining the binding affinity of the receptor-ligand pairs [138]. Accordingly, Xu et al. have derived the separation-dependent change in Gibbs free energy using the expression

$$\Delta G_{2D}(l) \approx U_0 - k_B T \ln\left(A_b/A\right) - k_B T \ln\left(\Omega_b \Omega_{RL}/\Omega_R \Omega_L\right) \qquad (6)$$

where A_b is the translational phase space area of the receptor-ligand complex, A is the area of the membrane, Ω_R (Ω_L) is the rotational phase space volume of the unbound receptors (ligands), and Ω_{RL} is the rotational phase space volume of the receptor-ligand complex. This latter term Ω_{RL} is given by

$$\Omega_{RL}(l) \simeq 2\pi \int_0^{\pi/2} \exp\left(-H_{RL}(\theta;l)/k_B T\right) \sin\left(\theta\right) d\theta, \qquad (7)$$

where $H_{RL}(\theta;l) \approx k_a \theta^2 + k_{RL}(l \sec(\theta) - L_0)^2$ is the contribution to the Hamiltonian due to anchoring and binding interactions of receptor-ligand complexes, θ is the angle between the membrane normal and the receptor (ligand) rod, k_a is the anchoring strength, k_{RL} is the spring-constant of the receptor-ligand complex, and L_0 is its preferred length (these last two parameters are determined from a combination of theory and MD data). The rotational phase space volume of the unbound receptors (ligands) Ω_R (Ω_L) is determined by an approach similar to Eq. (7), but is independent of the membrane separation ℓ. Similarly to the free-solution case, the separation-dependent binding affinity is given by

$$K_{2D}(l) = A \exp\left(-\Delta G_{2D}(l)/k_B T\right),$$

where, for thermally fluctuating membranes, the binding affinity can be determined by integrating against the probability distribution of membrane separations, as described by the equation

$$K_{2D} = \int K_{2D}(l)P(l)dl.$$

From MD data, Xu et al. found that the membrane separation is normally distributed, with $P(l) \propto \exp\left((l-\bar{l})^2/2\epsilon_\perp\right)$, where $\bar{l}$ is the mean membrane separation and $\epsilon_\perp$ is its standard deviation.

According to Eqs. (6) and (7), the binding affinity $K_{2D}(l)$ is maximal at some $l_0 \leqslant L_0$, an inequality that follows from the geometric constraint implicit in the $\ell/\cos(\theta)$ term as well as fact that $\sin(\theta)$ is monotonically increasing for $\theta \in [0, \pi/2]$. In order to directly investigate the effect of force on binding affinity, Xu et al. [139] leveraged this fact and used a harmonic approximation for the binding affinity, given by,

$$K_{2D}(l) = K_{\max} \exp\left[-\frac{k_{RL}(l-l_0)^2}{2k_BT}\right], \tag{8}$$

where $K_{\max}$ is the maximal binding affinity. Given that their model deals with variations in membrane separation, it was appropriate to use it to investigate the effects of compressive and tensile forces on binding affinity (in contrast to the Bell formalism which can be used to model the effect of force applied in any direction). For compressive/tensile forces, the membranes will be at equilibrium when the force applied to the membrane is equal to the force exerted by the receptor-ligand pairs. This was be expressed as a force-balance condition, given by

$$\sigma A = N_{RL} k_{RL}(l - l_0),$$

where σ is the force per unit area (stress) applied to the membrane and N_{RL} is the number of receptor-ligand complexes on the membrane. When combined with Eq. (A.6), it is possible to compute the force-dependent binding affinity $K_{2D}(\sigma)$ implicitly by evaluating $\sigma = \pm g(K_{2D})$, where g is a function. Numerical evaluation of this relation revealed that binding affinity is maximal for $\sigma = 0$ and decreases as the magnitude of σ increases. Moreover, this also revealed that there exists a critical stress threshold σ_c (where $\partial\sigma/\partial K_{2D} = 0$ and $\partial^2\sigma/\partial^2 K_{2D} < 0$) beyond which there is no solution for binding affinity. Beyond this critical stress, we cannot expect receptor-ligand pairs to form, and thus the membranes will either peel apart or collapse onto one another (i.e., $K_{2D} = 0$). The validity of these predictions was further investigated using simulations, where very good agreement between theory and simulations was confirmed for most cases. In particular, it was found that the effective critical stress observed in simulations is well-predicted for tensile forces (i.e., $\sigma_c^{\text{tensile}} \approx \sigma_c$) while it is always lower than the theoretical value for compressive force (i.e., $\sigma_c^{\text{compress}} < \sigma_c^{\text{tensile}}$). Through careful analysis of the critical stress for compressive forces, it was found that the deviations from theory could be well-explained by an Euler buckling instability.

Aside from pushing the boundaries of theoretical understanding of binding kinetics of transmembrane receptors, this theory gave some insights into the biophysical constraints that lead to adhesion release. At the rear of the cell, RhoA-dependent contractile stresses increase during the retraction of the trailing edge [140,141]. According to the theory covered here, this will lead to a decrease in the binding affinity of integrins (likely leading to a decrease in the size of FAs). If stress eventually surpasses the critical stress threshold, σ_c, all integrins in the FA will unbind leading to release of the adhesion.

In this section, we have seen how a force-balance condition for the membrane leads to the existence of a critical stress value, beyond which the transmembrane receptors cannot support the

applied force. Due to the intrinsic geometric aspects of the problem, it was treated as a fundamentally macroscopic problem with the theory developed only applicable to compressive and tensile forces. In Section 6, we will use a microscopic approach based on the Bell formalism developed in Section 3.2 that also predicts the existence of a critical force value and can be used to model the effects of sheer force as well.

5. Mechanically-driven clustering of integrins

The computational approach developed by Xu et al. (see Section 4, [138]) was also used to investigate the effect of the glycocalyx on integrin binding affinity as well as the spatial clustering it induces. The glycocalyx is a thin layer of anionic material that coats the cell and is made up of a network of glycoproteins and proteoglycans [142]. The glycocalyx has long been associated with the regulation of cell adhesion [143]. Moreover, Paszek et al. [144] recently found that metastatic tumors cells express an excess of large glycoproteins on their cell surface, and that the resulting thicker glycocalyx promotes clustering of integrins and adhesion formation. This finding had been predicted by a computational model previously developed by Paszek and collaborators [145]. Paszek's computational model explored numerical simulations of stochastically binding integrins with an extensive lattice spring model to account for membrane and ECM mechanics. They found that integrin clustering was due to an interplay between integrin binding affinity and glycocalyx repulsion [145]. Effectively, they proposed that a thick glycocalyx prevents integrin binding due to a large separation between the membrane and the ECM, while bound integrins will exclude thick glycoproteins from their vicinity, producing a kinetic trap where more integrins are likely to bind [144].

Due to membrane separation being a key factor in producing glycocalyx-driven integrin clustering, it seemed likely that the theory developed by Xu and collaborators (see Section 4) may be useful to understand this phenomenon. Indeed, in [139] Xu et al. modeled this integrin clustering phenomenon using their familiar system of rod-like receptors and ligands anchored to two apposing membranes, while simultaneously incorporating the effect of the glycocalyx by modeling it as a spring with a rest length of l_g and a stiffness per unit area of k_g. Using statistical mechanics methods, they then found that the separation between the two membranes is normally distributed, with a mean separation given by

$$\bar{l} = \frac{k_g A l_g + n k_b l_0 + \sigma A}{k_g A + n k_b}$$

and a standard deviation given by

$$\epsilon_\perp = \sqrt{k_B T / (k_g A + n k_b)}.$$

As can be seen in Eq. (8), the mean binding $K_{2D}(\bar{l})$ affinity is a monotonically decreasing function of l_g (or k_g). In view of the fact that a thicker glycocalyx will inevitably have a lower binding affinity than one for which $l_g \approx l_0$ (a prediction experimentally validated in [144]), it seems paradoxical that a thicker glycocalyx can enhance clustering. However, since clustering produces a different organization at local scales compared to global scales, the global binding affinity may not be adequate or even an appropriate tool to study this phenomenon. As an illustrative simplification of the problem at hand, let us consider the scenario in which the first successful bond has just been formed between a receptor-ligand pair. Near this receptor ligand pair, the membranes will be separated by a distance $l \approx l_0$ and thus, locally, the binding affinity can be approximated as

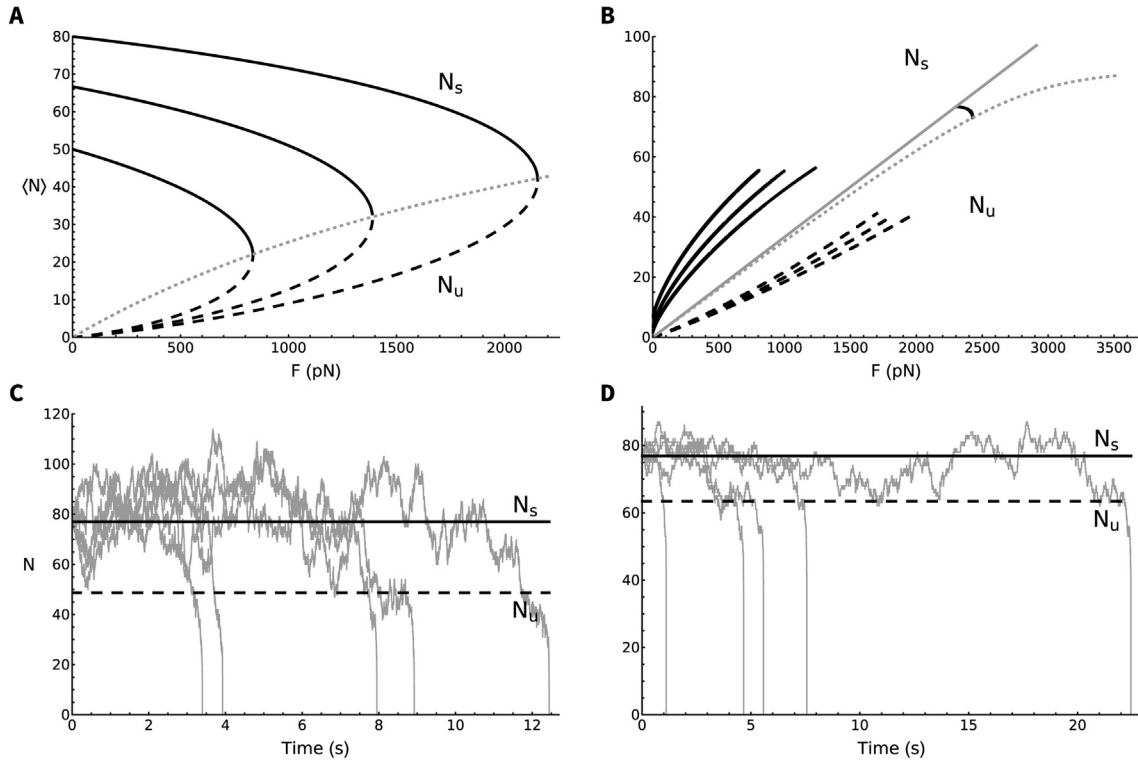$$K_{2D}(l \approx l_0) \approx K_{\max},$$

Fig. 3. Bifurcation analysis of the deterministic bond-cluster models reveals saddle-node bifurcations, explaining disassembly dynamics observed in stochastic realizations of these models. Bifurcation diagrams of the mean number of closed integrin-ligand bonds $\langle N \rangle$ with respect to the mechanical load applied to a cluster of bonds that share the load equally. Branches of stable (black solid lines labeled N_s) and unstable (black dashed lines labeled N_u) steady states meet at saddle-node bifurcation points. This feature is present in (A) the Bell model of adhesion using slip bonds, and (B) the Novikova model of adhesion using catch bonds. Gray dotted lines in A and B represent the set of all saddle-node bifurcation points obtained as the value of k_{on} is varied, while the grey solid line in B represents the set of all maximum points on N_s as the value of k_{on} is varied. In stochastic realizations of the models, if the system crosses the threshold determined by N_u all bonds will catastrophically unbind and the adhesion will disassemble. with respect to the mechanical load applied to a cluster of bonds that share the load equally. Branches of stable (black solid lines labeled N_s) and unstable (black dashed lines labeled N_u) steady states meet at saddle-node bifurcation points. This feature is present in (A) the Bell model of adhesion using slip bonds, and (B) the Novikova model of adhesion using catch bonds. Gray dotted lines in A and B represent the set of all saddle-node bifurcation points obtained as the value of k_{on} is varied, while the grey solid line in B represents the set of all maximum points on N_s as the value of k_{on} is varied. In stochastic realizations of the models, if the system crosses the threshold determined by N_s all bonds will catastrophically unbind and the adhesion will disassemble. Parameters used to compute the black curves are $N_t = 100$, $k_{off}^0 = 1\,s^{-1}$, $F_0 = \phi_{max}F_s = 30\,pN$, and $k_{on} = 1,2,4\,s^{-1}$ from bottom to top. Representative stochastic realizations of (C) the Bell model with $N_t = 290$, $k_{on} = k_{off}^0 = 1\,s^{-1}$, and $F \approx 2422\,pN$, as well as (D) the Novikova model with $N_t = 100$, $k_{on} = k_{off}^0 = 1\,s^{-1}$ and $F \approx 2306\,pN$, depicted as gray lines exhibiting catastrophic unbinding when $N \approx N_u$ (N_t was chosen in C such that the values of N_s are comparable in C and D). The black solid and dashed lines in C and D are the values of the N_s and N_u, respectively, highlighted in panels A and B.

while far-away from this receptor-ligand pair $l \approx l_g > l_0$ and the relevant binding affinity is

$$K_{2D}\left(l \approx l_g\right) \ll K_{max}.$$

Therefore, we will not only see more bonds form near an already-existing bond (as there is also a similar local enhancement of the binding rate k_{on} [146,139]) but also see these bonds more likely to remain formed compared to lone ones forming far away. Statistically, this leads to integrin clustering that is driven purely by mechanical considerations, that does not require the active generation of forces in the actin cytoskeleton. While a qualitative mechanistic understanding of this phenomenon can be obtained from the original computational model [145], the study by Xu et al. found excellent agreement between their own MD data and a theoretical framework based on Eq. (8) [139]. This demonstrated that their theoretical framework is generic enough to study diverse problems through analytic means as an alternative to numerical simulations which are non-trivial to implement.

6. Mechanical response of integrin clusters

We have thus far elucidated how the unbinding rates of single integrins vary with the applied force and how this relates to the conformational changes involved in activation, as well as how

force affects the binding affinity of a spatially distributed population of transmembrane receptors on a membrane. As we explained in the previous section, the mechanical effect of the glycocalyx helps to organize integrins into clusters by making local binding-dependent kinetic traps. Furthermore, adaptor proteins in the adhesion plaque locally slow the diffusion of integrins [36]; this as a result enhances the kinetic trapping of integrin underneath the plaque to produce a feed-forward system that leads to organization of integrins (and adaptor proteins) into discrete adhesions [132,35].

Therefore, it seems relevant to ask how these discrete adhesions, which consist of tens of integrin molecules that stochastically bind and unbind [36,16,147], are affected by the active forces generated in the actin cytoskeleton. This question was first investigated by Bell who modeled an adhesion as a collection of bonds sharing a fixed load while dynamically unbinding and rebinding [113]. For a cluster of slip bonds containing N_t integrins under a fixed load F, the mean number of closed bonds $\langle N \rangle$ to obeys the rate equation given by

$$\frac{d}{dt}\langle N \rangle = -\langle N \rangle k_{off}^0 \exp\left(F/(\langle N \rangle F_0)\right) + k_{on}(N_t - \langle N \rangle) \tag{9}$$

where $k_{off}^0 > 0$ is the unbinding rate in the absence of force, $k_{on} > 0$ is the binding rate of a single integrin, and F_0 is as defined in Eq. (3).

To characterize the long-term behaviour of such a model, one may seek steady states whose unbinding rate (first term in Eq. (9)) is equal to the binding rate (second term). Due to the fact that these rates are exponential and linear functions of $\langle N \rangle$, respectively, it is possible to obtain as many as two such states for $\langle N \rangle > 0$ [148]. In the scenario with two steady states, the elevated one has its load distributed over comparatively more bonds. This helps to explain why this elevated steady state is consistently found to be stable (see solid line in Fig. 3A), while the lower steady state is an unstable steady state (see black dashed line in Fig. 3A). When a bond is broken in the elevated steady state, denoted N_s, the increase in the unbinding rate (due to an increase in $F/\langle N \rangle$) is compensated by an increase in the binding rate (due to the increase in $N_t - \langle N \rangle$). When a bond is broken at the lower steady state, denoted N_u, however, the increase in the unbinding rate is larger than the corresponding increase in the binding rate and thus once a single bond breaks the cluster as whole catastrophically unbinds. As the force F is increased, the two steady states come closer to one another, until they annihilate at a critical force F_c determined by a saddle-node bifurcation (see grey dotted line in Fig. 3A) located at

$$F_c = F_0 N_t W\left[k_{on}/\left(k_{off}^0 e\right)\right], \tag{10}$$

where W is the Lambert W function (i.e., the product-log function). For $F > F_c$, no steady state exists with $\langle N \rangle > 0$; this means that, a cluster with a fixed number of bonds can only support up to a finite load that can be predicted using Eq. (10). This also highlights the importance of rebinding for the cluster to be able to resist applied forces, as in the absence of rebinding, we have $F_c \propto W(0) = 0$.

The deterministic treatment of the model suggests that once the system reaches a stable steady state, it will remain there indefinitely. However, one may wonder if stochastic effects, particularly when adhesions only have a few closed bonds, may alter this outcome. In order to answer such a question, in [149], Erdmann and Schwarz reformulated Eq. (9) in a discrete setting as a one-step master equation given by

$$\frac{d}{dt}p_i = r_{i+1}p_{i+1} + g_{i-1}p_{i-1} - (r_i + g_i)p_i, \tag{11}$$

where p_i is the probability of having i closed bonds, and r_i and g_i are bond rupture and gain rate functions, respectively, defined by

$$r_i = ik_{off}^0 \exp\left(F/(iF_0)\right) \text{ and } g_i = k_{on}(N_t - i).$$

Within this setting, we may define the lifetime of a cluster to be the expected time it takes for a stochastic processes described by Eq. (11) starting with N_t closed bonds to reach a state with zero closed bonds. Using standard results from the theory of Markov Chains [150,151], such a quantity may readily be computed

$$T = \sum_{i=1}^{N_t} \frac{1}{r_i} + \sum_{i=1}^{N_t-1}\sum_{j=i+1}^{N_t} \frac{\prod_{k=j-i}^{j-1} g_k}{\prod_{k=j-i}^{j} r_k}. \tag{12}$$

By evaluating this expression for $N_t \geqslant 2$, one obtains an expression that increases polynomially with respect to the binding rate, but decreases exponentially with respect to force. This is reminiscent of the difference we saw in the thermodynamic model of integrin activation, where the force-independent reaction had a much more limited effect compared to the force-dependent reaction. While the deterministic picture suggests that for $F < F_c$ the system will reach N_s provided that $N(t=0) > N_u$ and remain there indefinitely, a stochastic treatment of the problem shows that even for $N(t=0) = N_t > N_s > N_u$, the system will reach $N(t) = 0$ in finite time given by Eq. (12). Moreover, from the qualitative stability analysis described above, we may posit that for $F > 0$, the unstable steady state N_u acts as a threshold separating stochastic trajectories. If at any point in time an adhesion has (i) $N(t) < N_u$, it will

almost surely undergo catastrophic unbinding where all bonds unbind very quickly or (ii) $N(t) > N_u$ it will grow towards N_s until stochastic fluctuations cause the system to be in scenario (i) and disassemble. This perspective has indeed been confirmed using stochastic simulations (see Fig. 3C and D, and [129]).

As suggested before, integrin bonds exhibit a catch bond behaviour, but the models of bond-clusters investigated thus far have all assumed a slip bond for the integrin-ligand pair. In order to account for this, in [129], Novikova and Storm used Eq. (11) with an expression for r_i derived from the two-pathway model for catch bonds, given by Eq. (5) with $F_s = F_c$, and kept $g_i = k_{on}(N_t - i)$ as before to describe the system. Using mean field analysis, they were able to implicitly solve for the steady states of $\langle N \rangle$ from an expression for the total force applied to the adhesion, given by

$$F = F_s\langle N\rangle\phi_{max} \pm F_s\langle N\rangle\cosh^{-1}\left(\frac{k_{on}}{k_{off}^0}\frac{\alpha(N_t - \langle N\rangle)}{2\langle N\rangle}\right), \tag{13}$$

where $\phi_{max} > 0$ (a unitless parameter) determines the maximum bond lifetime as $F_s\phi_{max}$, and $\alpha > 0$ (also a unitless parameter) specifies the relative rates of the two pathways (according to the two-pathway interpretation of Eq. (5)). By plotting $\langle N \rangle$ versus F for both branches of Eq. (13), they obtained an elliptic-shaped curve with two (stable and unstable) branches that meet at a saddle-node bifurcation, leading to adhesion disassembly at large forces similar to the Bell model (see grey dotted line in Fig. 3B for various values of k_{on}). However, due to the increasing phase of the catch bond lifetime, the stable branch N_s increases significantly with applied force until it reaches a maximum value (highlighted by the grey solid line in Fig. 3B). This behaviour is strikingly different from what was seen for slip bonds where the stable branch N_s monotonically decreased with force (compare the solid black lines in Fig. 3A and B). This feature of the Novikova model thus gives a simple theoretical explanation for adhesion reinforcement, the observation that adhesions grow in response to applied force [18,31]. Interestingly, this latter model has very few closed bonds in the absence of force, implying that stable adhesions cannot form in the absence of significant force, which is at odds with experimental observations [152]. This discrepancy can be resolved by an appropriate change in parameters that abrogates the adhesion reinforcement phenomenon [129]. By considering the adhesion as a mixture of integrin heterodimers that contain either β_1 or β_3 subunits thatbehave as either catch or slip bonds, respectively [153,154], the bond-cluster model can be made to be mechanically resilient at low forces while maintaining its ability to reinforce at high forces [155].

7. Adhesion plaque formation

As discussed in Section 2.1, the adhesion plaque forms due to adsorption of adaptor proteins, resulting in the net growth of the adhesion. The plaque is an intrinsically dynamic structure, which continually exchanges matter with the cytosol [12,13,156,157]. At the molecular level, the dynamics of plaque assembly/disassembly appear to be related to the degree of aggregation of adaptor proteins, with the binding/unbinding of paxillin monomers to/from the plaque being associated with assembly while the unbinding of larger aggregates is associated with disassembly [12]. Interestingly, the size of adaptor protein aggregates observed in adhesions has been shown to be a biochemically regulated property that the cell can adjust through signaling pathways (e.g., phosphorylation events [158,157]). This paints a picture of a plaque made of adaptor proteins which not only bind to integrins, but also to one another, forming pleiomorphic ensembles with dynamic composition, size, and rapid turnover [159]. Regardless of what is known about adaptor protein dynamics at the molecular level, it is typical to characterize adhesion dynamics by a net assembly or

disassembly rate, depending on which phase of the adhesion life cycle is under consideration [160,19,161–163]. This provides a simplistic conceptual model with which we may understand plaque dynamics; a model that assumes that when the on-rate of adaptor proteins is larger than the off-rate adhesions will assemble, but when the reverse is true they disassemble. The experimental recordings of the different phases of the adhesion life cycle suggest that the net on- and off-rates of adaptor proteins varies in both space and time, and that adhesions do not seem to simply switch between assembly and disassembly, but also exhibit a plateau phase where adhesion size is roughly constant for some period of time [162,19].

From Eq. (A.7), we can see that the net adsorption process will reach equilibrium when μ_{agg}, the chemical potential of adaptor proteins in their aggregated state inside the adhesion, is equal to μ_{bulk}, their chemical potential in the cytosolic bulk. However, if one assumes that the adhesion plaque is a condensed phase of adaptor proteins with a fixed density and that the cytosol acts as a large bath of adaptor proteins (μ_{bulk} = constant), it is unclear how the system may reach equilibrium. By considering the geometric constraints of the adsorption process, Gov proposed a set of mathematical models which can explain the existence of the plateau phase observed during adhesion assembly as the system reaching equilibrium [164]. In contrast to the more common scenarios involving adsorption, where the binding sites for molecules are a preexisting feature of the liquid-solid interface, the binding sites for adaptor proteins are part of the adhesion itself. It is therefore necessary to consider the size and shape of the adhesion when quantifying its rate of growth. In order to do so, one must specify the region(s) where adsorption and desorption occur. Gov considered two possible regions; (i) the bulk of the adhesion, or (ii) the periphery of the adhesion [164].

By assuming that adsorption and desoprtion may not be symmetric, Gov derived four possible modes of growth for plaque dynamics: "Bulk-on/Bulk-off", "Bulk-on/End-off", "End-on/End-off", and "End-on/Bulk-off". For example, with a circular adhesion geometry, the "Bulk-on/Bulk-off" and "End-on/Bulk-off" models were given by $\frac{\partial A}{\partial t} = (k_{on} - k_{off})A$, and $\frac{\partial A}{\partial t} = k_{on}\sqrt{A/\pi} - k_{off}A$, respectively. The "Bulk-on/Bulk-off" model has no non-zero steady state, and the sign of $k_{on} - k_{off}$ determines whether the adhesion grows or shrinks exponentially in time. However, if a given adhesion grows arbitrarily large, the assumption of fixed μ_{bulk} will no longer be valid, and a steady state will be reached [132]. The "End-on/Bulk-off" model, on the other hand, has a steady state given by $\bar{A} = \pi(k_{on}/k_{off})^2$. This means that by either imposing the conservation of matter on a symmetric net adsorption process ("Bulk-on/Bulk-off") or by simply having an asymmetric net adsorption process ("End-on/Bulk-off"), the plaque reaches a steady state size. Although these models were applied to circular domains to describe adhesions, the results obtained for rectangular geometries were qualitatively the same [164]. Indeed, Gov showed that the rectangular geometry for FA produces the most compatible results with FA-size data provided that the "End-on/Bulk-off" ("End-on/End-off") model is considered when the FAs are small (large) [164]. The size-dependent switch in dynamics was interpreted as being reflective of the association of stable stress fibres to larger FAs which prevents loss of adaptor proteins through the bulk of the adhesions (i.e., the "Bulk-off" switches to "End-off" upon stress fibre association) [164].

While Gov's approach can explain the existence of the plateau phase during assembly, it does not explain the origin of disassembly. Within Gov's framework, the only way for disassembly to occur, after an adhesion reaches its plateau phase, is through an imposed change in adaptor protein adsorption kinetics (via the parameters k_{on} and k_{off}). Nascent adhesions disassemble quickly once they are no longer underneath the dense actin meshwork of the lamellipodium [19,54]. Therefore, it is possible that their disassembly directly reflects either an increased adaptor protein off-rate due to a decreased association with actin filaments [165], or a decrease in the availability of certain adaptor proteins that are delivered to NAs via diffusion along actin filaments (e.g., VASP [166]). Alternatively, in fibroblasts, an increased density of microtubule tips near the nucleus has been found to produce a gradual decrease in the size of mature FAs as they move rearward relative to the motion of the cell. This process is likely mediated by the endocytosis of integrins [63,59], where it is unclear to what extent adaptor proteins are also internalized. Interestingly, a modification of Gov's formalism accounting for the interaction between integrins and adaptor proteins could explain the decrease in FA-area through an integrin-dependent increase in k_{off} [132]. For mature FAs, however, it has also been shown that disassembly can be initiated by a decrease in applied mechanical force [161]. In the following section, we will explore a model that incorporates the mechanics of the adhesion plaque into kinetics of adsorption while accounting for mechanosensitive integrin activation, and see how forces can be used to regulate adhesion assembly and disassembly.

8. Mechanical response of the adhesion plaque

As the mechanical linkage between integrins and the actin-cytoskeleton, the adhesion plaque is subject to a number of mechanical forces which have been hypothesized to lead to biochemically-relevant deformation of adaptor proteins. In particular, it has been hypothesized that these deformations may underlie the phenomenon of adhesion sliding. The mathematical theory describing the mechanosensitivity of the adhesion plaque was pioneered by Nicolas, Safran, and collaborators in a number of studies [167,37–39,168,40]. Fundamentally, these studies focused on the mechanical response (i.e., deformation) of the adhesion plaque by treating it as an elastic thin film grafted onto the cytosol-membrane interface and subjecting it to shear forces [167]. The grafting boundary condition results in a force-balance equation, defined in one dimension by the following equation

$$k_0 a^2 \frac{d^2 u}{dx^2} - k_b u + F(x) = 0,$$

where u is the displacement of material due to the applied force, k_0 is the stiffness of the springs assumed to connect adjacent units in the plaque, a is a length-scale which characterizes the units, $k_b u$ is a restoring force caused by the connection between the fixed substrate and the adhesion (such that k_b is proportional to the stiffness of the composite integrin-adaptor-actin linkage), and $F(x)$ is an applied force. By considering a gate-like force applied just inside the adhesion's boundary, it was predicted that adhesion plaque material is compressed at the proximal tip of the adhesion while being expanded at its distal tip [167]. This prediction was then used to formulate a physically plausible mechanism for the anisotropic growth of adhesions in response to unidirectional force, whereby an unspecified "mechanosensitive unit" that constitutes the adhesion plaque responds to deformation through changes in its adsorption/desorption kinetics [37]. These kinetic changes are primarily understood through energetic considerations. For instance, in order for a mechanosensitive unit to be incorporated into a plaque under fixed stress it must bear some non-zero force, which will result in its deformation. By using Hooke's law, one can estimate the energetic cost of deformation using the equation $\Delta\mu_{el} \approx f^2 a^2/2k$, where f is the force per mechanosensitive unit, and k is a spring constant. While the cell is likely to have enough energy to deform these mechanosensitive units, in order to do so, they must be inside the plaque (i.e, adsorbed). The adsorption process (and subsequent

deformation) will thus occur spontaneously only if the elastic deformation energy is offset by a larger decrease in free energy due to the adsorption process. This means that, adsorption only occurs if

$$\Delta\mu_{agg}(f) = \Delta\mu_{el} - \Delta\mu_{chem} \approx \frac{f^2 a^2}{2k} - \Delta\mu_{chem}(f) < 0, \qquad (14)$$

where $\Delta\mu_{chem}$ is the intrinsic free energy change due to the adsorption of a single mechanosensitive unit. Nicolas and Safran assumed this change in free energy to be linearly proportional to the change in plaque density [37], and based on this deduced that at the proximal (compressed) tip, it is given by

$$\Delta\mu_{chem}(f) \approx e \frac{f}{\sqrt{kk_0}},$$

where e is the free energy of adsorption of a single unit ($e > 0$ for spontaneously forming adhesions). Implicit in this formulation is the assumption that the adhesion in question has reached its thermodynamic equilibrium prior to being loaded with force, since $\Delta\mu_{agg} = 0$ in the absence of the applied mechanical force. With these expressions, it is possible to investigate adhesion plaque dynamics once the applied force f is turned on. Since for $f \approx 0$, we have $\Delta\mu_{agg} < 0$ and that when $f \to \infty$ we have $\Delta\mu_{ads} \to \infty$, it follows that there exists a critical f^* satisfying

$$f^* = \frac{2e}{a^2 \sqrt{k_0/k}}$$

where $\Delta\mu_{agg}(f = f^*) = 0$ beyond which growth of the proximal tip becomes an unfavourable process. In order to refine the conditions for adhesion growth beyond the exothermic constraint defined by Eq. (14) Nicolas and Safran used Eq. (A.11) to determine v_+ and v_-, the rates of adsorption and desorption at the proximal and distal tips, respectively [37]. Subsequent analysis of the net adhesion growth rate (i.e., $v_+ - v_-$) revealed that, despite growth of the distal tip being energetically favourable for $f \approx 0$, the adhesion as a whole does not grow unless $0 \leqslant f_{min} < f < f_{max} < f^*$, while desorption at the distal tip dominates the growth process outside of this range. When, $f < f_{min}$, an adhesion will undergo resorption where it continually shrinks in size. For $f = f_{min}, f_{max}$, the desorption rate at the distal tip equals the adsorption rate at the proximal tip, representing a treadmilling regime for the plaque model where the adhesion is translocated towards the cell center while maintaining a constant size and remaining fixed to the substrate.

These results were expanded upon by Besser and Safran in a subsequent study, by considering the more biophysically-relevant scenario in which the plaque may be divided into two functionally distinct layers: the signaling layer and the force transduction layer [39]. The model in this study accounted for both the force-transmission through adaptor proteins in the transduction layer, as well as the force-induced activation of the mechanosensitive units in the signaling layer that could be due to (i) the expansion and compression of the plaque material (as was assumed by Nicolas and Safran [37]), or (ii) direct mechanical stretching of proteins (as had subsequently been predicted by Bruinsma [169]). In

their model, adsorption kinetics were also incorporated in a congruent manner through the use of the equation

$$\partial\phi/\partial t \propto \left(\mu_{bulk} - \mu_{agg}\right)$$

that describes the dynamics of the fractional adaptor protein concentration $0 < \phi(x,t) < 1$ in the condensed plaque phase [170]. Through the application of traveling wave solutions ($\phi(x,t) = \phi(x - vt)$), net adsorption rates of the distal and proximal tips of the adhesion were successfully computed and the existence of new modes of growth not previously found in the original model were discovered. One of these modes is the sliding resorption mode for $f < f_{min}^0 < f_{min}$ where adhesions shrink while being translocated in the direction of force. This approach, however, did not account for the energetic cost of deforming the plaque ($\Delta\mu_{el}$), leading to the prediction that adhesions will always grow at arbitrarily high forces.

This last point was resolved in a follow up study [40] that considered not only the intrinsic energy of plaque deformation $\Delta\mu_{el}$, but also the total energy of substrate deformation $H_{el}^{substrate}$. By using Eq. (A.16), it was shown that this latter consideration reduces the chemical potential μ_{agg} by a term that is proportional to the length of the adhesion and inversely proportional to the stiffness of the substrate (i.e., it vanishes for an infinitely rigid substrate). This allowed adhesions to have an equilibrium size, a feature that was lacking in previous iterations of the model. It also led to the very interesting prediction that both the equilibrium size and the adhesion's equilibration kinetics (i.e., the rate at which it reaches equilibrium) scale linearly with elastic modulus of the substrate (i.e., its stiffness). In other words, the model predicted that adhesion size grows linearly with the stiffness of the substrate, an outcome that was later been validated experimentally [171]. It is important, however, to note that this can only be true within a finite stiffness range as the finite size of the cell should prevent adhesions from growing indefinitely [172,173].

The modes of growth reported in the studies highlighted here (summarized in Table 1) were echoed in others [174,175], albeit with some differences in model formulation (see [150,175] for an in-depth discussion). Of particular interest, are the sliding resorption and sliding growth modes. The sliding resorption modes are likely to be relevant to the adhesion sliding phenomenon discussed in Section 2.2, while the sliding growth mode is likely to be relevant to adhesion maturation. The model presented in [40] predicted that the cell may switch between the two modes through an increase in the traction stress applied to adhesion. Traction forces are consistently higher at the retracting rear of migrating cells [140,176,141,177], where sliding FAs are primarily found [79,178,179], compared to their mid-bodies, where FAs are typically stationary relative to the ECM. Moreover, this model predicted that, the sliding growth mode is likely to have a significantly smaller sliding velocity compared to the high-force sliding resorption mode. This mode of growth may explain the slow treadmilling behaviour that can be observed near the

Table 1
Summary of the different sliding modes predicted in Fig. 4A of [155].

Plaque Behaviour	Distal Tip	Proximal Tip	Sliding Velocity	Mechanical Condition
Resorption	$\longrightarrow$	$\leftarrow$	Negligible	$f < f_{min}^0$
Sliding Resorption	$\longrightarrow$	$\rightarrow$	Negligible	$f_{min}^0 < f < f_{min}$
Treadmilling	$\rightarrow$	$\rightarrow$	Negligible	$f = f_{min}$
Sliding Growth	$\rightarrow$	$\rightarrow$	Negligible-Moderate	$f_{min} < f < f_{max}$
Treadmilling	$\rightarrow$	$\rightarrow$	Near Maximal	$f = f_{max}$
Sliding Resorption 2	$\longrightarrow$	$\rightarrow$	Maximal-Moderate	$f_{max} < f < f_{max}^0$
Resorption	$\longrightarrow$	$\leftarrow$	Moderate	$f_{max}^0 < f$

protrusive regions of motile cells where FAs typically mature [19,180,181].

Finally, while we have focused on force as the variable that can lead to adhesion sliding, it is important to note that the force thresholds that determine the growth mode of the cell and its sliding velocity can all be modified biochemically. For instance, by increasing the free energy change of adaptor protein adsorption, ϵ_B, we can expect the force threshold for the sliding resorption growth modes to increase; similar effects can be expected when increasing λ_{xz}, the rigidity of the integrin-adaptor-actin linkage (equivalent to k discussed previously in relation to [37]). The effect of the force-insensitive inactivation of LFA-1 (i.e., loss of affinity regulation by force) at the rear of neutrophils as seen in [77] may be understood as the limit when $\tau \to 0$, where τ is the force-sensitivity of the integrin activation energy barrier. By decreasing τ, the sliding velocity can be made arbitrarily small, suggesting that modulation of integrin force-sensitivity (either through biochemical modifications or through switching integrin subunits) may induce adhesion release by not only weakening the integrin-ECM bond but also by halting the movement of sliding adhesions. Furthermore, decreasing ϵ_B causes a decrease in both the sliding and growth velocities of the adhesion. Such a change in ϵ_B could be due to cleavage of bonds by proteases (e.g., calpain), suggesting that protease activity may have similar effect to the loss of affinity regulation on adhesion release. This body of work thus provided important insights into how the relative energetic contributions of biochemical reactions and mechanical deformation manifest themselves in the kinetics of adsorption/desorption and produce physiologically-relevant adhesion dynamics.

9. Mechanical response of the membrane

Building upon the success of the adhesion plaque models developed by Nicolas and collaborators, the long-range mechanical response of a membrane containing integrins was investigated by Xu and collaborators [182]. Their work did not explicitly consider the presence of FAs on the membrane, but focused on the activation, subsequent ligand-binding, and internalization of integrins on the membrane and how these processes are modulated by ECM stiffness. Similar to previous work [169,40,104], they used a force-dependent energy difference between inactive and active conformations of integrin, given by

$$\Delta\mu_{act} = \mu^0 - F\Delta x,$$

where μ^0 is the intrinsic energy difference between the active and inactive conformations in the absence of force, F is the magnitude of the sheer force applied to the integrin, and Δx is the length difference that characterizes the conformational change. The force per integrin was determined by modeling the membrane as ribbon lying on an elastic ECM; under such assumptions the force varies is space [183], and is given by

$$F(x) \propto f_t \exp(-x/\lambda_T),$$

where f_T is the membrane tension at the leading edge and λ_T is a space-constant determined by the relative material stiffness of the ribbon (i.e., the composite system of membrane, integrins, and adaptors) and ECM as well as their heights [182]. The probability of integrin activation was computed using a Boltzmann factor, given by

$$p_{act} = \left(1 + \exp\left[\Delta\mu_{act}/k_BT\right]\right)^{-1}$$

or

$$p_{act}(x) = \left(1 + \exp\left[(\mu^0 - F(x)\Delta x)/k_BT\right]\right)^{-1}.$$

This effectively predicts activation probability is close to unity near the leading edge and remains roughly constant until it drops off to zero at some finite distance inside the cell. Due to the dependence of λ_T on ECM stiffness, Xu et al. found that the finite length at which activation drops off decreases with increasing ECM stiffness, indicating that more integrins can be activated on a softer ECM. Assuming that integrins must be activated to bind, they modeled the binding probability by considering two opposing effects (i) the release of energy ($U < 0$) due to receptor-ligand binding and (ii) the stretching of integrins by the force f_c that caveolin exerts on the membrane [184]. Accounting for both of these effects, the probability of an integrin being bound was found to be

$$p_{bound} = p_{act}\left(1 + \exp\left[\left(U + f_c^2/2k_{eff}\right)/k_BT\right]\right)^{-1},$$

where k_{eff} is the effective stiffness of the composite integrin-ECM system and is given by $k_{eff}^{-1} = k_I^{-1} + k_M^{-1}$ with k_I (k_M) being the stiffness of integrin receptors (ECM). The term $f_c^2/2k_{eff}$ quantifies the deformation energy induced by caveolin, which becomes arbitrarily large as $k_M, k_I \to 0$. On ECMs of all stiffness, $p_{bound} \propto p_{act}$; however, the constant of proportionality decreases on softer ECMs, suggesting that soft ECMs counter-intuitively favor both activation and unbinding. The force of caveolin on the membrane will only induce internalization if it is energetically favourable to do so. Xu et al. used a theory of invagination, developed by Sens and Turner in [184], to derive an exothermic condition for the internalization of the membrane (and any integrin present). By accounting for the energy of the integrins on the pre-internalized membrane, they were able to express this energetic condition as a function of p_{bound}, subsequently concluding that internalization occurs if $p_{bound} < p_c$, with $p_c \approx 0.25$ in the physiological parameter regime. These and previous results thus show that p_{bound} is consistently lower on a softer ECM, implying that a softer ECM will always exhibit more internalization. This dual effect of ECM stiffness on integrins may explain why bone marrow mesenchymal stem cells exhibit both increased integrin activation and internalization on soft matrices [185].

10. Comparison of model outcomes

Thus far, we have touched on two broad classes of adhesion models, bond-cluster models (see Section 6 [186,149,148,129,155]) and adhesion-plaque models (see Section 8 [167,37,38,40]). Although these two classes of models differ in their construction, they both predict that adhesions can grow in size in response to force, and that beyond a critical force value, the adhesion will begin to disassemble. They also produce predictions that are inconsistent with each other. More specifically:

1. Bond-cluster models always predict an adhesion with finite size at zero force, while the mechanosensitive plaque models presented above suggest that there may exist a threshold in force required to produce adhesions. This is a consequence of the fact that bond-cluster models do not consider the dynamics of adaptor proteins, whereas the mechanosensitive plaque models suggest that adsorption becomes kinetically favourable only once force crosses a threshold.
2. In the adhesion-plaque models, disassembly is caused by a switch in net adsorption kinetics to favour desorption, but they consider that their adaptor protein-integrin complexes may become arbitrarily stretched (which is unlikely to be valid for large forces). On the other hand, in the bond-cluster models, disassembly is due to mechanical breakage of integrin bonds.

In order to remedy this, bond-cluster models should account for the kinetics of adsorption while the plaque models should account for the force-dependent unbinding of integrin-ligand bonds. The former can be accomplished by explicitly tracking the growth of the plaque, and making the binding of integrins somehow dependent on the plaque size, while the latter may be implemented by assuming that, as integrin bonds become broken, the desorption of nearby adpator proteins will become overwhelmingly favoured.

11. A hybrid model

The bond-cluster models and adhesion-plaque models assume the presence of either adaptor proteins or integrins, respectively, and investigate the dynamics of the other class of proteins. As noted in Section 2, these two classes of proteins cooperate to form the adhesion and its associated cytoskeletal structures (F-actin and stress fibres). Based on this, in order to analyze adhesion dynamics, it seems imperative to model the cooperation between these two major types of proteins that make up the adhesion. Previous models that have taken into account both protein classes to study adhesions have either implicitly or explicitly assumed that adpator proteins and integrins form complexes with a 1:1 ratio, implying that the fluxes of the two proteins into or out of the adhesion are identical [175,187]. This assumption is difficult to reconcile with the observation that integrin density within different FAs can vary by 3-fold in the same cell, whereas adaptor protein densities vary less and they have a characteristic pair-wise distance that is conserved across adhesion classes [81,188,189]. One exception to this modeling choice was the mechanosensitive model developed by Besser and Safran [39] (and subsequently augmented with energetic terms from Nicolas and Safran [40]), in which the force transmitted to integrins was hypothesized to be proportional to the local density of adaptor proteins (see above). In contrast to experimental observations, however, this model assumed that integrins are already organized as a template for the adhesion plaque to grow on [35,19]. A model of nascent adhesions developed by MacKay and Khadra [132] resolved this issue, by explicitly specifying the spatial and binding dynamics of integrins and the adsorption kinetics of adaptor proteins, and generated a model that allowed for a variable density of integrins inside the adhesion.

The variable integrin-density model [132] has made a number of important contributions to the theoretical understanding of NAs. Firstly, as suggested by Fig. 3 A and B, there is always an unstable steady state N_u between the elevated stable steady state N_s and the single molecule initial condition $N = 1$ (for $F > 0$). This makes it unclear as to how adhesions can assemble in the presence of force given that their trajectory through state space to N_s will always be impeded by N_u. Novikova and Storm took note of this issue and posited that in order to observe assembly in their model, it is necessary to consider the time-dependent force that results from assembly/contraction of stress fibres [129]. Indeed, the inclusion of a time-dependent forces did allow Walcott et al. to produce assembly starting from a single molecular complex when stochastically simulating the model [187]. Markedly, this latter model was too complex to allow for mean field analysis of the full system. To resolve this issue, Walcott et al. performed this analysis on a one-variable reduced system and found that it possesses a configuration of steady states equivalent to the bond-cluster models discussed above (i.e., $0 < N_u < N_s$). It remained, however, unclear how their model overcomes the aforementioned issue with the unstable steady state (or the saddle fixed point in the high dimensional state space Walcott et al. used in producing the stochastic simulations). MacKay and Khadra [132], on the other hand, performed their mean field analysis on their full three-variable model, ensuring that the saddle fixed point (N_u) remains relevant to the dynamics of the model while allowing the system more degrees of freedom to bypass it. Consistent with previous studies, they found that under fixed load, adhesions do not assemble for $F > 0$ when $N_u > 0$, as they are kinetically trapped by the stable manifold of the saddle. Unlike previous studies on bond-cluster models in which it was only possible to specify adhesion load [186,149,129,155], the explicit modeling of the adhesion plaque in MacKay and Khadra [132] allowed them to define not only the load on the adhesion but also the stress. Indeed, with a fixed value of stress, they demonstrated that one can obtain adhesion-assembly from an initial condition consisting of a single integrin-adaptor protein complex, suggesting that stress is the permissive mechanical parameter which allows for assembly when $F, N_u > 0$. Thus, while the formation and contraction of a stress fibre is a physiologically-relevant origin for the force exerted on adhesions [168,187], any dynamic model which results in a force that grows linearly with adhesion area should be able to produce assembly from a single molecule initial condition.

It should be mentioned here that MacKay and Khadra [132] have identified a parameter regime (labeled region 2) in which N_u is negative, making the stable manifold of the saddle no longer
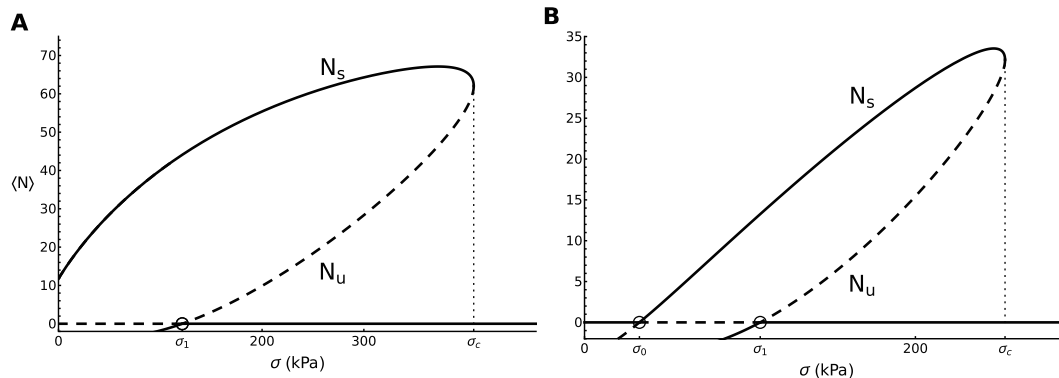

Fig. 4. Bifurcation analysis of the deterministic hybrid model by MacKay and Khadra [132] in "region 2" of parameter space. Bifurcation diagrams of the number of closed integrin-ligand bonds $\langle N \rangle$ with respect to mechanical stress applied on NAs when the integrin-ligand binding rate is A) 5.9 s^{-1}, and B) 0.18 s^{-1}. Solid lines represent branches of stable steady states, whereas dashed lines represent branches of saddle fixed points. The two elevated branches of stable steady states and saddle fixed points labeled N_s and N_u, respectively, merge at saddle-node bifurcation points at a given critical stress σ_c in both A and B. These two branches also intersect the lower branch of trivial steady states $(A, \langle N \rangle, \langle M \rangle) = (0,0,0)$, where A ($\langle M \rangle$) is the area of the adhesion (the mean number of mobile integrins inside the adhesion), at transcritical bifurcation points (open circles) only once in A at $\sigma = \sigma_1$ and twice in B at $\sigma = \sigma_0 > 0$ and $\sigma = \sigma_1 > \sigma_0$. As a result, NAs exhibit finite adhesion size at zero force in A while NAs do not form in the absence of force in B (i.e., no clustered solution). Notice that for $\sigma \in [0, \sigma_1]$ in A and for $\sigma \in [\sigma_0, \sigma_1]$ in B, adhesions starting at $\langle N \rangle \approx 0$ can freely reach the stable steady state N_s (compare to Fig. 3 where no such region exists), and that force must cross a threshold σ_0 in B in order for NAs to assemble (as in the model by Nicolas and Safran [37]).

an obstacle for adhesion assembly (see Fig. 4). Within this region, it was possible to reach $N_s > 0$ regardless of the mechanical conditions imposed on the adhesion (Fig. 4). There are no equivalent parameter regimes in previously published models of bond-clusters [186,149,148,129,155] that could produce this type of behaviour. Interestingly, within this region one may find that adhesions will not form unless force (either load or stress) crosses a threshold (see Fig. (4)B). This finding reconciles the differences in model outcomes between the bond-cluster and mechanosensitive adhesion-plaque models. Moreover, due to the explicit modeling of the adhesion plaque by MacKay and Khadra [132], the disassembled state ($\langle N \rangle = 0$) is a well-defined equilibrium in their mean field analysis (compare Figs. 3 and 4), whereas in previous models of bond-clusters, it was not and the behaviour of the system close to or beyond the saddle-node bifurcation had to be verified through stochastic simulations. It should be mentioned here that the model by MacKay and Khadra further assumed a relation between the net adsorption rate of adpator proteins and the density of integrins under the plaque [132]. This means that, upon collective integrin bond failure (at high forces), integrins will diffuse away, and the adhesion plaque will dissolve as a consequence. This is in contrast to the mechanosensitive adhesion-plaque models where adaptor proteins may be arbitrarily stretched at high forces. Thus, by jointly considering the dynamics of integrins and adaptor proteins, this newly developed model is a hybrid one that shares characteristics with both classes of models: the bond-cluster model and the mechanosensitive adhesion-plaque model.

12. Conclusions and outlook

Focal adhesions are intrinsically dynamic structures which, for a long time, have fascinated biologists and physicists alike. The explosion of data related to focal adhesions in the past two decades has greatly assisted in delineating of the structural makeup of adhesions as well as the dynamics and interactions governing adhesions. At the single molecule level, the biochemical and mechanical steps involved in integrin activation are reflected in the mechanosensitive properties of the integrin-ligand bond [105,102]. These mechanical properties have been used to build theoretical models of adhesions as cluster of bonds that fail beyond a critical load [113,186,148,129]. Alternatively, the deformation of the adhesion plaque in response to applied mechanical force can be used to understand the complex sliding behaviour that adhesions exhibit [18,17,37,40]. While these models have some fundamental differences in their predictions, recent work has helped to bridge this gap and explain how adhesions can form in the presence of mechanical forces [132].

While the combination of experimental data and theoretical modeling has been quite fruitful in explaining the mechanisms underlying some experimental observations, a number of unexplored phenomena remain. Nascent adhesions have not received as much attention as other more mature classes of adhesions, including FAs, either from an experimental or theoretical point of view. In fact, some theorists have suggested that they exist only transiently as their formation is intrinsically thermodynamically unfavourable [37,173]. Recent experimental findings have cast doubt on this notion, where NAs have been found to be stable for hundreds of seconds on supported lipid bilayers [152]. Moreover, membrane tension and buckling instabilities in the actin meshwork of the lamellipodium have recently emerged as the driving force which triggers NA formation [190,191]. Although a theoretical framework to understand this has been outlined [53], it seems that it has not directly led to the formulation of a mathematical framework to describe it. This represents a challenging problem to tackle in a mathematically tractable manner as one must con-

sider the temporal buildup of force, movement of the leading edge relative to the adhesions, as well as the assembly of the adhesion.

Although the mechanical properties of the integrin-ligand bond has been incorporated into a number of models, it is worth noting that it is not the only mechanosensitive bond present in the adhesion. Indeed, talin has been found to exhibit a weak slip bond while vinculin produces a stronger catch bond when bound to actin [192,193]. Thus far, adhesion-plaque models have treated adaptor proteins rather generically [164,175,187,173,194,132,37,40], despite extensive characterization of their biochemical and biophysical properties [41,15,12,158,195,49,157,196,163]. For instance, it is known that the binding dynamics of the adaptor protein paxillin is asymmetric along an adhesion and that these binding dynamics are likely related to phosphorylation events that are associated with highly dynamic adhesions (i.e., sliding adhesions) [195,49,163]. In addition, the bio-mechanically regulated vertical movement of adaptor proteins within the adhesion, such as the translocation of vinculin from the signaling layer to the transduction layer in response to changes in paxillin phosphorylation [15], has generally been neglected. Together, these effects, combined with vinculin's ability to reinforce the talin-actin bond, may provide a molecularly explicit mechanism for the plaque's mechanical response (a feature missing in the mechanosensitive plaque models developed thus far). With the large number of possible interactions, it may be challenging to keep such a model mathematically tractable while capturing the experimental observations. The force of the glycocalyx is likely to also induce conformational changes (e.g., activation) in integrin receptors [144]. While integrin activation and inactivation were indeed considered in the original computational model of glycocalyx-driven clustering by Paszek et al., these processes were modeled as being force-independent. Not surprisingly, activation was not found to influence clustering. However, it has been shown that not only activation is force-dependent (see Section 8), but also that the repulsive forces coming from the glycocalyx can indeed activate integrins [144]. Given that integrin binding affinity strongly influences this clustering [145], the relative contribution of the mechanosensitive integrin-ligand bond in glycocalyx-driven clustering remains unclear.

While most integrins exhibit the catch bond behaviour when presented with an appropriate ligand [125,134,136,197], there are some differences in the force-lifetime relationship of these bonds. Moreover, it seems to have been previously thought that integrin heterodimers containing β_1 subunits behaved as catch bonds whereas those with β_3 subunits behave as slip bonds [198]. The idea that the mechanosensitive properties of the integrin bond are determined by the β subunit is logical, as it is the β subunit which associates with the actin cytoskeleton [83]. However, it was recently shown that $\alpha_V \beta_3$ integrins behave as a catch bond when presented with fibronectin under the right chemical conditions [197,135], and as a slip bond when presented with for its a physiologically relevant ligand Thy-1 [199]. This highlights the complex interplay between chemical environment and ligand-specificity that determine the mechanosensitive properties of the integrin bond. Further theoretical investigation of the determinants of mechanosensitive properties of these bonds should be undertaken in order to understand how the integrin-ligand bond varies its catch bond properties and may be switched from a catch bond to a slip bond. An approach that uses thermodynamic considerations similar to [104] with a kinetic model similar to [102] may indeed be fruitful in this endeavour. Furthermore, the consequences of having a membrane populated by multiple integrin heterodimers remains relatively unexplored, with the exception of [155].

Another very interesting avenue for research is the bi-directional relation between biochemical signaling pathways

regulating motility and adhesions. Rho GTPases such as Cdc42, Rac, and Rho are the drivers of cell migration, and the biochemical pathways that exert their control over the cell are subject to modulation by adhesion-dependent signaling [200–202]. Numerous models have been developed to account for the Rac-Rho signaling pathway responsible for establishing the cell polarity necessary for directed motility [203,204,23,24]. While this polarization mechanism can be influenced by adhesion-dependent signaling pathways [23,168], its influence on the mechanical state of the actin cytoskeleton [168] as well as adhesion-regulatory biochemical pathways [23] suggest that adhesion dynamics are also influenced by Rac-Rho signaling. Due to the bi-directional positive feedback between the two systems, it remains unclear to what extent these effects on adhesion dynamics are mechanical or biochemical in nature. Mathematical modeling may help to answer these questions as, in principle, it allows one to decouple the two effects from each other.

Cell migration is also regulated by a polarized gradient in calcium (Ca^{2+}) concentration and/or activity [205], exhibiting an increasing gradient from the front of a motile cell to the rear. These spatiotemporal activities are regulated by Ca^{2+} fluxes across the membrane, such as through stretch-activated channels (e.g., TRPV4 and TRPM7 channels) and numerous other pumps/receptors (for more details, see the review by Wei et al. [206]). Moreover, it has been observed that external mechanical stimulation results in mechanosensitive channel activation primarily in the vicinity of FAs, suggesting that these tension-sensing proteins are activated by membrane tension that builds up around FAs. Noting that both membrane tension and mechanosensitive channel activity are elevated at the leading edge of motile cells [206,207,53], this suggests that there is a link between adhesions and Ca^{2+} dynamics in the context of motility. It has been suggested that the calpain family of intracellular Ca^{2+}-dependent proteases plays a key role in regulating cell migration [208,72,209,210], through their ability in modulating adhesion dynamics [211]. A number of adaptor proteins have been identified as targets for this protease, including talin, focal adhesion kinase (FAK) and paxillin [42]. Thus, the adhesion-dependent influx of Ca^{2+} through mechanosensitive channels is likely to have direct effect on adhesion dynamics. It remains unclear, however, how various Ca^{2+}-dependent signaling pathways interact at the cellular level to control adhesion assembly/disassembly through adaptor protein dynamics while maintaining the gradient in migrating cells. Although there is a wealth of studies analyzing Ca^{2+} handling in many cell-lines, this area continues to be largely unexplored mathematically in motile cells, which would provide insights into the role of Ca^{2+} in regulating cellular polarity and motility. Such studies will be crucial in elucidating the molecular coordination and propagation of Ca^{2+} signaling, particularly at the leading edge of the cell, the link between Ca^{2+} signaling, adhesions and membrane tension during migration and the role Ca^{2+} signaling in regulating collective migration.

CRediT authorship contribution statement

Laurent MacKay: Conceptualization, Formal analysis, Investigation, Methodology, Validation, Visualization, Writing - original draft, Writing - review & editing. **Anmar Khadra:** Funding acquisition, Resources, Supervision, Writing - review & editing.

Declaration of Competing Interest

The authors declare that they have no known competing financial interests or personal relationships that could have appeared to influence the work reported in this paper.

Acknowledgments

Appendix A. Thermodynamics and reaction kinetics

The set of models of adhesion dynamics covered in this article may seem to employ quite different mathematical approaches to study their dynamics. However, the vast majority of these models can understood through a common framework that is based on thermodynamics. This framework uses the notion of a potential, where a system tends to evolve from a high potential state to a low potential state. The notion of a potential has been generalized to chemical systems through the intrinsic thermodynamic quantity: "chemical potential". In this appendix we will derive an expression for the chemical potential in dilute solutions, show how it relates to chemical kinetic reaction rates, and extend the definition beyond dilute solutions to include the effects of mechanical deformation.

A.1. Derivation of chemical potentials for dilute solutions

The thermodynamic quantity crucial for understanding biochemical dynamics is the free energy of a system; it represents the work that can be extracted from a system by accounting for energy loss through entropic heat production. In particular, biochemical systems are typically isothermal and isobaric and thus they are well described by the Gibbs free energy $G|_{P,T} = U + PV - TS$, where U is the internal energy of the system, P is its pressure, V is its volume, T is its temperature, and S is its entropy [212]. The differential form of the Gibbs free energy is given by

$$
\begin{aligned}
dG = & \ dU + d(PV) - d(TS) \\
= & \ VdP - SdT + \sum_i \mu_i dN_i
\end{aligned}
\tag{A.1}
$$

where μ_i is the chemical potential of the ith species in the system defined as $\mu_i = \partial G/\partial N_i|_{P,T}$, and N_i is the number of particles of the ith species in the system [212].

From Eq. (A.1), we can compute the change in free energy from a reference state with pressure P_0 to another state with pressure P_1, keeping the number of particles and temperature remain fixed

$$
\Delta G|_{T,N} = \int_{P_0}^{P_1} VdP.
$$

Using the ideal gas law, $PV = NRT$ (where $N \equiv N_i$ is the number of molecules of the ith species and P is the partial pressure of that species), we can rewrite this as

$$
\Delta G|_{T,N} = NRT \int_{P_0}^{P_1} \frac{dP}{P} = NRT \ln (P_1/P_0).
\tag{A.2}
$$

This means that the chemical potential can be computed by taking the partial derivative of Eq. (A.2) with respect to N while keeping the pressure ($P = P_1$) and temperature (T) fixed. Together with the ideal gas law, these conditions imply that the concentration is a conserved quantity in the system, i.e.,

$$\left.\begin{array}{l} \frac{\partial P}{\partial N} = 0 \\ \frac{\partial T}{\partial N} = 0 \\ P_1 V_1 = N k_B T \end{array}\right\} \Rightarrow \frac{\partial}{\partial N}\left(\frac{N}{V_1}\right) = 0 \Longleftrightarrow \frac{N}{V_1} = C = \text{constant},$$

which is equivalent to saying that

$$\Delta G|_{P,T} \equiv \Delta G|_{C,T} = NRT \ln(C/C_0), \tag{A.3}$$

where C_0 is the concentration at the reference state. Using Eq. (A.3), we can then compute an expression for chemical potential from its definition, as follows

$$\begin{aligned} \mu_i = \frac{\partial G}{\partial N_i}\big|_{P,T} &= \frac{\partial \Delta G|_{C,T}}{\partial N_i} \\ &= RT\ln(C) \underbrace{-RT\ln(C_0)}_{\mu^0} \\ &\rightleftharpoons \mu(C) = \mu^0 + RT\ln(C), \end{aligned} \tag{A.4}$$

where μ^0 is referred to as the standard chemical potential. Eq. (A.4) provides a relationship between chemical potential and concentration by approximating the a dilute solution as an ideal gas (i.e., using the equation of state $PV = NRT$). For systems with a different equation of state one can obtain other formulations for the chemical potential. For example, the Van der Waals equation may be used to derive an alternative equation for $\mu(C)$ for non-ideal gases [213].

In our derivations, we have made reference to some arbitrary reference states. In the next subsection, we will show that in dilute solutions undergoing chemical reactions, these reference states are not entirely arbitrary but reflect the intrinsic kinetics of the reactions taking place.

A.2. Standard chemical potentials and the law of mass action

Let us first consider a dilute solution undergoing a set of elementary chemical reactions (to be distinguished from composite reactions [214]) whose jth reaction is expressed as

$$\sum_i \alpha_{i,j} X_i \underset{k_j^-}{\overset{k_j^+}{\rightleftharpoons}} \sum_i \beta_{i,j} X_i, \tag{A.5}$$

where X_i is the ith chemical species in the system, $\alpha_{i,j}$ ($\beta_{i,j}$) is the stochiometric coefficient of X_i as a reactant (product) in the jth reaction, and k_j^+ (k_j^-) is the forward (reverse) rate constant of the jth reaction. According to the law of mass action [151,215], at equilibrium this reaction is characterized by a relationship, given by

$$\frac{\prod_i \overline{C}_i^{\alpha_{i,j}}}{\prod_i \overline{C}_i^{\beta_{i,j}}} = \frac{k_j^-}{k_j^+},$$

or equivalently

$$\prod_i \overline{C}_i^{\,\nu_{i,i}} = K_j, \tag{A.6}$$

where $\{\overline{C}_i\}$ are the equilibrium concentrations, $\nu_{i,j} = \alpha_{i,j} - \beta_{i,j}$ is the net stochiometric coefficient of the ith species in the jth reaction, and $K_j = k_j^-/k_j^+$ is the equilibrium constant for the jth reaction. By considering a closed isothermal and isobaric system at thermodynamic equilibrium (i.e. $dG = dP = dT = 0$), we may obtain from Eq. (A.1)

$$\sum_i \mu_i dN_i = 0.$$

For a closed system, fluctuations in N_i can only be due to the elementary reactions and thus

$$dN_i = \sum_j \nu_{i,j} d\chi_j$$

where χ_j is the extent of reaction for the jth reaction [214]. This implies that

$$\sum_i \mu_i \sum_j \nu_{i,j} d\chi_j = \sum_j d\chi_j \sum_i \mu_i \nu_{i,j} = 0$$

which can only hold for arbitrary $d\chi_j$ if

$$\sum_i \mu_i \nu_{i,j} = 0, \qquad \forall j. \tag{A.7}$$

We note that this is the equilibrium condition relating the chemical potentials of chemical species undergoing elementary reaction. Using Eq. (A.4), we can rewrite this last expression as

$$\begin{aligned} -\sum_i \mu_i^0 \nu_{i,j} &= \sum_i RT\ln\left(\overline{C}_i\right)\nu_{i,j}, \\ &= RT\ln\left(\prod_i \overline{C}_i^{\,\nu_{i,j}}\right), \end{aligned}$$

where we can identify the product inside the logarithm as the left hand side of Eq. (A.6). Based on this we may finally write the relationship between standard chemical potentials and the equilibrium constant as

$$\sum_i \mu_i^0 \nu_{i,j} = -RT\ln(K_j), \qquad \forall j \tag{A.8}$$

which provides one constraint on the set $\{\mu_i^0\}$ for each reaction considered.

A.2.1. Application to an isomerization reaction

Consider the isomerization reaction

$$A \underset{k^-}{\overset{k^+}{\rightleftharpoons}} B,$$

where a molecules of A react to create one molecule of B. According to the definition of the standard chemical potential, $\mu_i^0 = -k_B T \ln\left(C_i^0\right)$ where C_i^0 is the concentration of the ith species at an arbitrary reference state (see Eq. (A.4)). From Eq. (A.8), we have a condition which relates this reference state to the equilibrium constant of a reaction. In particular, for the isomerization reaction, we have

$$-RT\ln\left(C_A^0\right) + RT\ln\left(C_B^0\right)$$

where $K = k^-/k^+$. By arbitrarily choosing $C_B^0 = 1$, we find that $C_A^0 = K$ and that the chemical potentials for A and B are given by

$$\mu_A(C_A) = RT\ln(C_A/K), \tag{A.9}$$

and

$$\mu_B(C_B) = RT\ln(C_B), \tag{A.10}$$

respectively.

A.3. Kinetic rates

The calculation of reaction rates is a fundamental problem encountered in many fields of science; for molecular systems, these reactions are typically understood as the thermally-assisted escape from metastable states (e.g., the molecular state A in the isomerization reaction) [216]. The basic formalism can be derived from the empirical Van't Hoff-Arrhenius law [217,218], given by

$$r = k \exp\left(-\Delta E^{\ddagger}/RT\right),$$

where r is the rate of escape, k is a pre-exponential factor, and $\Delta E^{\ddagger} = E_{\ddagger} - E_1$ is the activation energy which characterizes the energy difference between the metastable state (denoted by 1) and the transition state (denoted by $\ddagger$). The computation of the pre-exponential factor k from first principles has been the subject of much research, with different formalisms producing nuanced predictions that are challenging to verify in biochemical reactions [216]. Nonetheless, it has been found that a consistent thermodynamic formulation may be obtained by taking

$$r = k^0 \exp\left(-\left(\mu_{\ddagger}^0 - \mu_1\right)/RT\right), \tag{A.11}$$

where $\mu_{\ddagger}^0$ is the concentration-independent intrinsic molar free energy of the transition state, and $k^0 > 0$ is a kinetic prefactor [219,220]. For single molecules, we simply have $\mu_1 = \mu_1^0$, whereas for dilute solutions undergoing reactions, the chemical potential of the reactant and product state of the jth reaction are given by $\mu_{1,j} = \sum_i \alpha_{i,j}\mu_i$ and $\mu_{2,j} = \sum_i \beta_{i,j}\mu_i$, respectively, where μ_i is given by Eq. (A.4) with μ_i^0 determined according to Eq. (A.8). According to this view of chemical kinetics, the forward and backward rates are given by

$$r_j^+ = k_{j,+}^0 \exp\left[-\left(\mu_{\ddagger j}^0 - \mu_{1,j}\right)/RT\right],$$

and

$$r_j^- = k_{j,-}^0 \exp\left[-\left(\mu_{\ddagger j}^0 - \mu_{2,j}\right)/RT\right],$$

respectively, where $k_{j,-}^0$ and $k_{j,+}^0$ are positive parameters and $\mu_{\ddagger j}^0$ is the intrinsic free energy of the transition state for the jth reaction. By noting that Eq. (A.7) (the condition for thermal equilibrium) can be rewritten as

$$\mu_{1,j} = \mu_{2,j}$$

and that, at thermodynamic equilibrium, we must have $r_j = r_j^+ - r_j^- = 0$, we may conclude that $k_{j,-}^0 = k_{j,+}^0$. In the case of the isomerization reaction described above, the choice $k_+^0 = k_-^0 = k_- \exp\left(\mu_0^{\ddagger}/RT\right)$ yields the net rate

$$r = k^+ C_A - k^- C_B, \tag{A.12}$$

which is consistent with the law of mass action [215]. This suggests that free energy of the transition state has already been implicitly included in the chemical potential of the reactive dilute solution through Eq. (A.8). Nonetheless, it is important to consider Eq. (A.11) for a system whose the equilibrium constant for a given reaction (K_j) may be tuned by a free parameter θ (e.g. applied force), as the equations $\mu_{1,j}^0(\theta) = \sum_i \alpha_{i,j}\mu_i^0(\theta)$, $\mu_{2,j}^0(\theta) = \sum_i \beta_{i,j}\mu_i^0(\theta)$ and $\mu_{\ddagger j}^0(\theta)$ will determine how each reaction rate varies with θ. Thus, Eq. (A.11) provides us with a single formalism describes the non-equilibrium rates of reaction at both micro- and macroscopic scales.

A.4. Applications to mechanochemistry

Within the context of mechanochemistry, various scenarios can arise requiring the knowledge of how μ varies with pressure (or applied force). This can be done by fixing the temperature and pressure and computing the change in Gibbs free energy during an increase in the number of particles in the system from N_0 to N, given by

$$\Delta G|_{T,P} = \int_{N_0}^{N} \mu(N')dN'.$$

As we saw in Appendix A.1, the condition of fixed pressure and temperature is equivalent to fixing the concentration, with $\mu(N) = \mu$, implying that

$$\Delta G|_{T,P} = \mu(N - N_0).$$

The latter can be used to compute the total differential of the Gibbs free energy

$$dG|_{T,P} = d\mu N + \mu dN. \tag{A.13}$$

Equating Eqs. (A.1) and (A.13), we arrive at the Gibbs-Duhem equation

$$Nd\mu = VdP - SdT. \tag{A.14}$$

Systems are typically assumed to be under isothermal conditions ($dT = 0$), allowing us to compute the force-dependent chemical potential, given by

$$\mu(P) = \int \frac{V(P)}{N(P)} dP. \tag{A.15}$$

This approach was used by Hill to derive a force-dependent chemical potential for the subunits that make up microtubules, modeling microtubules as one dimensional elastic polymers [221]. In this one dimensional polymer setting, we may use the negative applied force $-F$ (rather than P) and the length per monomer l (rather than V/N) [221]. Using Hooke's law, the force on a subunit of length l is given by

$$F = k(l - l_0),$$

where k is a spring constant and l_0 is the rest length of of the subunit. Substituting $l = l_0 + F/k$ into Eq. (A.15), we obtain

$$\begin{aligned} \mu(F) = \; & \mu_0 - \int (l_0 + F/k)dF \\ = \; & \mu_0 - l_0 F - F^2/2k. \\ \simeq \; & \mu_0 - l_0 F \end{aligned}$$

This example not only illustrates how force affects the chemical potential (and thus influences reaction rates), but also provides an expression that can be used to model the effect of applied force on adhesion plaque molecules in linear focal adhesions [174,222]. On the other hand, if mass is not homogeneous but is characterized by a particle density $N(x)$, the Gibbs free energy can be written as a functional, given by

$$G = \int_V g(x, N(x), \nabla N(x))dV,$$

and the chemical potential can be computed pointwise by taking the functional derivative

$$\mu(x) = \frac{\delta G}{\delta N} = \frac{\partial g}{\partial N} - \nabla \cdot \frac{\partial g}{\partial \nabla N}. \tag{A.16}$$

This approach thus allows us to consider situations beyond those that can be dealt with using the Gibbs-Duhem equation. Indeed, Safran and collaborators have used it to quantify the non-trivial relationship between a material science description of plaque deformation and the kinetics of adsorption which produce the plaque [38–40].

References

[1] Lo CM, Wang HB, Dembo M, Wang YL. Cell movement is guided by the rigidity of the substrate. Biophys J 2000;79(1):144–52. https://doi.org/10.1016/S0006-3495(00)76279-5. URL: http://www.ncbi.nlm.nih.gov/pubmed/10866943, http://www.pubmedcentral.nih.gov/articlerender.fcgi?artid=PMC1300921, http://www.pubmedcentral.nih.gov/articlerender.fcgi?artid=1300921&tool=pmcentrez&rendertype=abstract.
[2] Devreotes P, Janetopoulos C. Eukaryotic chemotaxis: distinctions between directional sensing and polarization. J Biol Chem 2003;278(23):20445–8.

https://doi.org/10.1074/jbc.R300010200. URL: http://www.ncbi.nlm.nih.gov/pubmed/12672811.

[3] Engler AJ, Sen S, Sweeney HL, Discher DE. Matrix elasticity directs stem cell lineage specification. Cell 2006;126(4):677–89. https://doi.org/10.1016/j.cell.2006.06.044. URL: http://www.ncbi.nlm.nih.gov/pubmed/16923388.

[4] Huselstein C, De Isla N, Kolopp-Sarda MN, Kerdjoudj H, Muller S, Stoltz JF. Influence of mechanical stress on cell viability. Biorheology 2006;43:371–5. URL: http://www.ncbi.nlm.nih.gov/pubmed/16912409.

[5] Fu J, Wang YK, Yang MT, Desai RA, Yu X, Liu Z, Chen CS. Mechanical regulation of cell function with geometrically modulated elastomeric substrates. Nat Methods 2010;7(9):733–6. https://doi.org/10.1038/nmeth.1487. URL: http://www.nature.com/articles/nmeth.1487.

[6] Brás-Pereira C, Moreno E. Mechanical cell competition. Curr Opin Cell Biol 2018;51:15–21. https://doi.org/10.1016/J.CEB.2017.10.003. URL: https://www.sciencedirect.com/science/article/pii/S0955067417300765.

[7] Friedl P, Gilmour D. Collective cell migration in morphogenesis, regeneration and cancer. Nat Rev Mol Cell Biol 2009;10(7):445–57. https://doi.org/10.1038/nrm2720. URL: http://www.nature.com/doifinder/10.1038/nrm2720.

[8] Luster AD, Alon R, von Andrian UH. Immune cell migration in inflammation: present and future therapeutic targets. Nat Immunol 2005;6(12):1182–90. https://doi.org/10.1038/ni1275.

[9] Li L, He Y, Zhao M, Jiang J. Collective cell migration: Implications for wound healing and cancer invasion. Burns Trauma 2013;1(1):21–6. https://doi.org/10.4103/2321-3868.113331. URL: http://www.ncbi.nlm.nih.gov/pubmed/27574618, http://www.pubmedcentral.nih.gov/articlerender.fcgi?artid=PMC4994501.

[10] Kucik DF, Dustin ML, Miller JM, Brown EJ. Adhesion-activating phorbol ester increases the mobility of leukocyte integrin LFA-1 in cultured lymphocytes. J Clin Invest 1996;97(9):2139–44. https://doi.org/10.1172/JCI118651. URL: http://www.ncbi.nlm.nih.gov/pubmed/8621804, http://www.pubmedcentral.nih.gov/articlerender.fcgi?artid=PMC507289.

[11] Brown CM, Hebert B, Kolin DL, Zareno J, Whitmore L, Horwitz AR, et al. Probing the integrin-actin linkage using high-resolution protein velocity mapping. J Cell Sci 2006;119(Pt 24):5204–14. https://doi.org/10.1242/jcs.03321.

[12] Digman MA, Brown CM, Horwitz AR, Mantulin WW, Gratton E. Paxillin dynamics measured during adhesion assembly and disassembly by correlation spectroscopy. Biophys J 2008;94(7):2819–31. https://doi.org/10.1529/biophysj.107.104984. URL: http://www.sciencedirect.com/science/article/pii/S0006349508705332.

[13] Wolfenson H, Lubelski A, Regev T, Klafter J, Henis YI, Geiger B. A role for the juxtamembrane cytoplasm in the molecular dynamics of focal adhesions. PLoS ONE 2009;4(1): . https://doi.org/10.1371/journal.pone.0004304. URL: http://www.ncbi.nlm.nih.gov/pubmed/19172999, http://www.pubmedcentral.nih.gov/articlerender.fcgi?artid=PMC2627934e4304.

[14] Morimatsu M, Mekhdjian AH, Adhikari AS, Dunn AR. Molecular tension sensors report forces generated by single integrin molecules in living cells. Nano Lett 2013;13(9):3985–9. https://doi.org/10.1021/nl4005145.

[15] Case LB, Baird MA, Shtengel G, Campbell SL, Hess HF, Davidson MW, Waterman CM. Molecular mechanism of vinculin activation and nanoscale spatial organization in focal adhesions. Nat Cell Biol 2015;17(7):880–92. https://doi.org/10.1038/ncb3180. URL: http://www.ncbi.nlm.nih.gov/pubmed/26053221.

[16] Tsunoyama TA, Watanabe Y, Goto J, Naito K, Kasai RS, Suzuki KG, Fujiwara TK, Kusumi A. Super-long single-molecule tracking reveals dynamic-anchorage-induced integrin function. Nat Chem Biol 2018;14(5):497–506. https://doi.org/10.1038/s41589-018-0032-5.

[17] Balaban NQ, Schwarz US, Riveline D, Goichberg P, Tzur G, Sabanay I, Mahalu D, Safran S, Bershadsky A, Addadi L, Geiger B, et al. Force and focal adhesion assembly: a close relationship studied using elastic micropatterned substrates. Nat Cell Biol 2001;3(5). https://doi.org/10.1038/35074532. URL: http://www.ncbi.nlm.nih.gov/pubmed/11331874.

[18] Riveline D, Zamir E, Balaban NQ, Schwarz US, Ishizaki T, Narumiya S, Kam Z, Geiger B, Bershadsky AD. Focal contacts as mechanosensors: externally applied local mechanical force induces growth of focal contacts by an mDia1-dependent and ROCK-independent mechanism. J Cell Biol 2001;153 (6):1175–86. URL: http://www.ncbi.nlm.nih.gov/pubmed/11402062, http://www.pubmedcentral.nih.gov/articlerender.fcgi?artid=PMC2192034.

[19] Choi CK, Vicente-Manzanares M, Zareno J, Whitmore LA, Mogilner A, Horwitz AR. Actin and alpha-actinin orchestrate the assembly and maturation of nascent adhesions in a myosin II motor-independent manner. Nat Cell Biol 2008;10(9):1039–50. https://doi.org/10.1038/ncb1763. URL: http://www.ncbi.nlm.nih.gov/pubmed/19160484, http://www.pubmedcentral.nih.gov/articlerender.fcgi?artid=PMC2827253.

[20] Bershadsky A, Kozlov M, Geiger B. Adhesion-mediated mechanosensitivity: a time to experiment, and a time to theorize. Curr Opin Cell Biol 2006;18 (5):472–81. https://doi.org/10.1016/j.ceb.2006.08.012. URL: http://www.ncbi.nlm.nih.gov/pubmed/16930976, http://linkinghub.elsevier.com/retrieve/pii/S0955067406001232.

[21] Chen B-C, Legant WR, Wang K, Shao L, Milkie DE, Davidson MW, Janetopoulos C, Wu XS, Hammer JA, Liu Z, English BP, Mimori-Kiyosue Y, Romero DP, Ritter AT, Lippincott-Schwartz J, Fritz-Laylin L, Mullins RD, Mitchell DM, Bembenek JN, Reymann A-C, Böhme R, Grill SW, Wang JT, Seydoux G, Tulu US, Kiehart DP, Betzig E. Lattice light-sheet microscopy: Imaging molecules to embryos at high spatiotemporal resolution. Science 2014;346(6208):1257998. https://doi.org/10.1126/science.1257998. URL: http://www.ncbi.nlm.nih.gov/pubmed/25342811, http://www.pubmedcentral.nih.gov/articlerender.fcgi?artid=PMC4336192.

[22] Jonkman JEN, Cathcart JA, Xu F, Bartolini ME, Amon JE, Stevens KM, Colarusso P. An introduction to the wound healing assay using live-cell microscopy. Cell Adhes Migration 2014;8(5):440–51. https://doi.org/10.4161/cam.36224. URL: http://www.ncbi.nlm.nih.gov/pubmed/25482647, http://www.pubmedcentral.nih.gov/articlerender.fcgi?artid=PMC5154238.

[23] Tang K, Boudreau CG, Brown CM, Khadra A. Paxillin phosphorylation at serine 273 and its effects on Rac, Rho and adhesion dynamics. PLoS Comput Biol 2018;14(7): . https://doi.org/10.1371/journal.pcbi.1006303e1006303.

[24] Lyda JK, Tan JZ, Rajah A, Momi A, MacKay L, Brown CM, Khadra A. Rac activation is key to cell motility and directionality: an experimental and modelling investigation. Comput Struct Biotechnol J [in Press]..

[25] Ananthakrishnan R, Ehrlicher A. The forces behind cell movement. Int J Biol Sci 2007;3(5):303–17. URL: http://www.ncbi.nlm.nih.gov/pubmed/17589565, http://www.pubmedcentral.nih.gov/articlerender.fcgi?artid=PMC1893118.

[26] Case LB, Waterman CM. Integration of actin dynamics and cell adhesion by a three-dimensional, mechanosensitive molecular clutch. Nat Cell Biol 2015;17 (8):955–63. https://doi.org/10.1038/ncb3191.

[27] Geiger B, Yamada KM. Molecular architecture and function of matrix adhesions. Cold Spring Harbor Perspect Biol 2011;3(5). https://doi.org/10.1101/cshperspect.a005033. URL: http://www.ncbi.nlm.nih.gov/articlerender.fcgi?artid=3101841&tool=pmcentrez&rendertype=abstract.

[28] Geiger B, Bershadsky A. Exploring the neighborhood: adhesion-coupled cell mechanosensors. Cell 2002;110(2):139–42. https://doi.org/10.1016/s0092-8674(02)00831-0. URL: http://www.ncbi.nlm.nih.gov/pubmed/12150922.

[29] Giannone G, Dubin-Thaler BJ, Rossier O, Cai Y, Chaga O, Jiang G, Beaver W, Döbereiner H-G, Freund Y, Borisy G, Sheetz MP. Lamellipodial actin mechanically links myosin activity with adhesion-site formation. Cell 2007;128(3):561–75. https://doi.org/10.1016/j.cell.2006.12.039. URL: http://www.ncbi.nlm.nih.gov/pubmed/17289574, http://www.pubmedcentral.nih.gov/articlerender.fcgi?artid=PMC5219974, https://linkinghub.elsevier.com/retrieve/pii/S0092867407001110.

[30] Oakes PW, Beckham Y, Stricker J, Gardel ML. Tension is required but not sufficient for focal adhesion maturation without a stress fiber template. J Cell Biol 2012;196(3):363–74. https://doi.org/10.1083/jcb.201107042. URL: http://www.ncbi.nlm.nih.gov/pubmed/22291038, http://www.pubmedcentral.nih.gov/articlerender.fcgi?artid=PMC3275371, http://www.jcb.org/lookup/doi/10.1083/jcb.201107042.

[31] Roca-Cusachs P, del Rio A, Puklin-Faucher E, Gauthier NC, Biais N, Sheetz MP. Integrin-dependent force transmission to the extracellular matrix by α)actinin triggers adhesion maturation. Proc Natl Acad Sci USA 2013;110 (15):E1361–70. https://doi.org/10.1073/pnas.1220723110. URL: http://www.pubmedcentral.nih.gov/articlerender.fcgi?artid=3625291&tool=pmcentrez&rendertype=abstract, http://www.ncbi.nlm.nih.gov/pubmed/23515331, http://www.pubmedcentral.nih.gov/articlerender.fcgi?artid=PMC3625291.

[32] Gardel ML, Sabass B, Ji L, Danuser G, Schwarz US, Waterman CM. Traction stress in focal adhesions correlates biphasically with actin retrograde flow speed. J Cell Biol 2008;183(6):999–1005. https://doi.org/10.1083/jcb.200810060. URL: http://www.ncbi.nlm.nih.gov/pubmed/19075110, http://www.pubmedcentral.nih.gov/articlerender.fcgi?artid=PMC2600750.

[33] Zaidel-Bar R, Itzkovitz S, Ma'ayan A, Iyengar R, Geiger B. Functional atlas of the integrin adhesome. Nat Cell Biol 2007;9(8):858–67. https://doi.org/10.1038/ncb0807-858. URL: http://www.ncbi.nlm.nih.gov/pubmed/17671451, http://www.pubmedcentral.nih.gov/articlerender.fcgi?artid=PMC2735470, http://www.nature.com/doifinder/10.1038/ncb0807-858, http://www.pubmedcentral.nih.gov/articlerender.fcgi?artid=2735470&tool=pmcentrez&rendertype.

[34] Springer TA, Dustin ML. Integrin inside-out signaling and the immunological synapse. Curr Opin Cell Biol 2012;24(1):107–15. https://doi.org/10.1016/j.ceb.2011.10.004. URL: http://www.ncbi.nlm.nih.gov/pubmed/22129583, http://www.pubmedcentral.nih.gov/articlerender.fcgi?artid=PMC3294052.

[35] Wiseman PW, Brown CM, Webb DJ, Hebert B, Johnson NL, Squier JA, Ellisman MH, Horwitz AF, et al. Spatial mapping of integrin interactions and dynamics during cell migration by Image Correlation Microscopy. J Cell Sci 2004;117 (23). URL: http://jcs.biologists.org/content/117/23/5521.long.

[36] Rossier O, Octeau V, Sibarita JB, Leduc C, Tessier B, Nair D, Gatterdam V, Destaing O, Albigès-Rizo C, Tampé R, Cognet L, Choquet D, Lounis B, Giannone G. Integrins β 1 and β 3 exhibit distinct dynamic nanoscale organizations inside focal adhesions. Nat Cell Biol 2012;14(10):1057–67. https://doi.org/10.1038/ncb2588. URL: http://www.nature.com/articles/ncb2588.

[37] Nicolas A, Geiger B, Safran SA. Cell mechanosensitivity controls the anisotropy of focal adhesions. Proc Natl Acad Sci 2004;101(34):12520–5. https://doi.org/10.1073/pnas.0403539101.

[38] Nicolas A, Safran SA. Limitation of cell adhesion by the elasticity of the extracellular matrix. Biophys J 2006;91(1):61–73. https://doi.org/10.1529/biophysj.105.077115. URL: http://www.ncbi.nlm.nih.gov/pubmed/16581840, http://www.pubmedcentral.nih.gov/articlerender.fcgi?artid=PMC1479082.

[39] Besser A, Safran SA. Force-induced adsorption and anisotropic growth of focal adhesions. Biophys J 2006;90(10):3469–84. https://doi.org/10.1529/BIOPHYSJ.105.074377. URL: https://www.sciencedirect.com/science/article/pii/S0006349506725292.

[40] Nicolas A, Besser A, Safran SA. Dynamics of cellular focal adhesions on deformable substrates: consequences for cell force microscopy. Biophys J 2008;95(2):527. https://doi.org/10.1529/BIOPHYSJ.107.127399. URL: http://www.ncbi.nlm.nih.gov/pubmed/18408038, http://www.pubmedcentral.nih.gov/articlerender.fcgi?artid=PMC2440452.

[41] Kanchanawong P, Shtengel G, Pasapera AM, Ramko EB, Davidson MW, Hess HF, Waterman CM. Nanoscale architecture of integrin-based cell adhesions. Nature 2010;468(7323):580–4. https://doi.org/10.1038/nature09621. URL: http://www.ncbi.nlm.nih.gov/pubmed/21107430, http://www.pubmedcentral.nih.gov/articlerender.fcgi?artid=PMC3046339.

[42] Brown M, Turner CE. Paxillin: adapting to change. Physiol Rev 2004;84(4):1315–39. https://doi.org/10.1152/physrev.00002.2004.

[43] Mitra SK, Hanson DA, Schlaepfer DD. Focal adhesion kinase: in command and control of cell motility. Nat Rev Mol Cell Biol 2005;6(1):56–68. https://doi.org/10.1038/nrm1549. URL: http://www.nature.com/articles/nrm1549.

[44] Critchley DR. Biochemical and structural properties of the integrin-associated cytoskeletal protein talin. Annu Rev Biophys 2009;38:235–54. https://doi.org/10.1146/annurev.biophys.050708.133744. URL: http://www.ncbi.nlm.nih.gov/pubmed/19416068.

[45] Dumbauld DW, Lee TT, Singh A, Scrimgeour J, Gersbach CA, Zamir EA, Fu J, Chen CS, Curtis JE, Craig SW, García AJ, et al. How vinculin regulates force transmission. Proc Natl Acad Sci USA 2013;110(24):9788–93. https://doi.org/10.1073/pnas.1216209110. URL: http://www.ncbi.nlm.nih.gov/pubmed/23716647, http://www.pubmedcentral.nih.gov/articlerender.fcgi?artid=PMC3683711.

[46] Atherton P, Stutchbury B, Wang D-Y, Jethwa D, Tsang R, Meiler-Rodriguez E, Wang P, Bate N, Zent R, Barsukov IL, Goult BT, Critchley DR, Ballestrem C. Vinculin controls talin engagement with the actomyosin machinery. Nat Commun 2015;6(1):10038. https://doi.org/10.1038/ncomms10038. URL: http://www.nature.com/articles/ncomms10038.

[47] Hirata H, Tatsumi H, Sokabe M. Mechanical forces facilitate actin polymerization at focal adhesions in a zyxin-dependent manner. J Cell Sci 2008;121(17):2795–804. https://doi.org/10.1242/jcs.030320. URL: http://www.ncbi.nlm.nih.gov/pubmed/18682496.

[48] Smith MA, Blankman E, Gardel ML, Luettjohann L, Waterman CM, Beckerle MC. A Zyxin-mediated mechanism for actin stress fiber maintenance and repair. Develop Cell 2010;19(3):365–76. https://doi.org/10.1016/j.devcel.2010.08.008. URL: https://www.sciencedirect.com/science/article/pii/S1534580710003837.

[49] Zaidel-Bar R, Milo R, Kam Z, Geiger B. A paxillin tyrosine phosphorylation switch regulates the assembly and form of cell-matrix adhesions. J Cell Sci 2006;120(1):137–48. https://doi.org/10.1242/jcs.03314. URL: http://www.ncbi.nlm.nih.gov/pubmed/17164291.

[50] Sun Z, Lambacher A, Fässler R. Nascent adhesions: from fluctuations to a hierarchical organization. Curr Biol 2014;24(17):R801–3. https://doi.org/10.1016/j.cub.2014.07.061. URL: http://www.sciencedirect.com/science/article/pii/S0960982214009300.

[51] Small J, Stradal T, Vignal E, Rottner K. The lamellipodium: where motility begins. Trends Cell Biol 2002;12(3):112–20. https://doi.org/10.1016/S0962-8924(01)02237-1.

[52] Mogilner A, Oster G. Cell motility driven by actin polymerization. Biophys J 1996;71(6):3030–45. https://doi.org/10.1016/S0006-3495(96)79496-1. URL: http://www.ncbi.nlm.nih.gov/pubmed/8968574, http://www.pubmedcentral.nih.gov/articlerender.fcgi?artid=PMC1233792.

[53] Keren K, Shemesh T. Buckle up: membrane tension drives lamellipodial network compression and adhesion deposition. J Cell Biol 2017;216(9):2619–21. https://doi.org/10.1083/jcb.201706111. URL: http://www.ncbi.nlm.nih.gov/pubmed/28765363, http://www.pubmedcentral.nih.gov/articlerender.fcgi?artid=PMC5584188.

[54] Thievessen I, Thompson PM, Berlemont S, Plevock KM, Plotnikov SV, Zemljic-Harpf A, Ross RS, Davidson MW, Danuser G, Campbell SL, Waterman CM. Vinculin-actin interaction couples actin retrograde flow to focal adhesions, but is dispensable for focal adhesion growth. J Cell Biol 2013;202(1):163–77. https://doi.org/10.1083/jcb.201303129. URL: http://www.ncbi.nlm.nih.gov/pubmed/23836933, http://www.pubmedcentral.nih.gov/articlerender.fcgi?artid=PMC3704983.

[55] Schober M, Raghavan S, Nikolova M, Polak L, Pasolli HA, Beggs HE, Reichardt LF, Fuchs E. Focal adhesion kinase modulates tension signaling to control actin and focal adhesion dynamics. J Cell Biol 2007;176(5):667–80. https://doi.org/10.1083/jcb.200608010. URL: http://www.ncbi.nlm.nih.gov/pubmed/17325207, http://www.pubmedcentral.nih.gov/articlerender.fcgi?artid=PMC2064024.

[56] Ballestrem C, Erez N, Kirchner J, Kam Z, Bershadsky A, Geiger B. Molecular mapping of tyrosine-phosphorylated proteins in focal adhesions using fluorescence resonance energy transfer. J Cell Sci 2006;119(5):866–75. https://doi.org/10.1242/jcs.02794. URL: http://www.ncbi.nlm.nih.gov/pubmed/16478788, http://jcs.biologists.org/cgi/doi/10.1242/jcs.02794.

[57] von Wichert G, Haimovich B, Feng G-S, Sheetz MP. Force-dependent integrin-cytoskeleton linkage formation requires downregulation of focal complex dynamics by Shp2. EMBO J 2003;22(19):5023–35. https://doi.org/10.1093/emboj/cdg492. URL: http://www.ncbi.nlm.nih.gov/pubmed/14517241, http://www.pubmedcentral.nih.gov/articlerender.fcgi?artid=PMC204475.

[58] Vicente-Manzanares M, Zareno J, Whitmore L, Choi CK, Horwitz AF. Regulation of protrusion, adhesion dynamics, and polarity by myosins IIA and IIB in migrating cells. J Cell Biol 2007;176(5):573–80. https://doi.org/10.1083/jcb.200612043. URL: http://www.ncbi.nlm.nih.gov/pubmed/17312025, http://www.pubmedcentral.nih.gov/articlerender.fcgi?artid=PMC2064016 https://rupress.org/jcb/article/176/5/573/34522/Regulation-of-protrusion-adhesion-dynamics-and.

[59] Rid R, Schiefermeier N, Grigoriev I, Small JV, Kaverina I. The last but not the least: the origin and significance of trailing adhesions in fibroblastic cells. Cell Motility Cytoskeleton 2005;61(3):161–71. https://doi.org/10.1002/cm.20076.

[60] Ilić D, Kovacic B, Johkura K, Schlaepfer DD, Tomasević N, Han Q, Kim J-B, Howerton K, Baumbusch C, Ogiwara N, Streblow DN, Nelson JA, Dazin P, Shino Y, Sasaki K, Damsky CH. FAK promotes organization of fibronectin matrix and fibrillar adhesions. J Cell Sci 2004;117(Pt 2):177–87. https://doi.org/10.1242/jcs.00845. URL: http://www.ncbi.nlm.nih.gov/pubmed/14657279.

[61] Efimov A, Schiefermeier N, Grigoriev I, Ohi R, Brown MC, Turner CE, Small JV, Kaverina I. Paxillin-dependent stimulation of microtubule catastrophes at focal adhesion sites. J Cell Sci 2008;121(3). https://doi.org/10.1242/jcs.03497. pp. 405–405.

[62] Bershadsky A, Chausovsky A, Becker E, Lyubimova A, Geiger B. Involvement of microtubules in the control of adhesion-dependent signal transduction. Curr Biol 1996;6(10):1279–89. https://doi.org/10.1016/S0960-9822(02)70714-8.

[63] Kaverina I, Krylyshkina O, Small JV. Microtubule targeting of substrate contacts promotes their relaxation and dissociation. J Cell Biol 1999;146(5):1033–44. https://doi.org/10.1083/jcb.146.5.1033. URL: https://rupress.org/jcb/article/146/5/1033/32015/Microtubule-Targeting-of-Substrate-Contacts.

[64] Ezratty EJ, Partridge MA, Gundersen GG. Microtubule-induced focal adhesion disassembly is mediated by dynamin and focal adhesion kinase. Nat Cell Biol 2005;7(6):581–90. https://doi.org/10.1038/ncb1262. URL: http://www.nature.com/articles/ncb1262.

[65] Chao W-T, Kunz J. Focal adhesion disassembly requires clathrin-dependent endocytosis of integrins. FEBS Lett 2009;583(8):1337–43. https://doi.org/10.1016/j.febslet.2009.03.037.

[66] Ezratty EJ, Bertaux C, Marcantonio EE, Gundersen GG. Clathrin mediates integrin endocytosis for focal adhesion disassembly in migrating cells. J Cell Biol 2009;187(5):733–47. https://doi.org/10.1083/jcb.200904054. URL: https://rupress.org/jcb/article/187/5/733/35702/Clathrin-mediates-integrin-endocytosis-for-focal.

[67] De Franceschi N, Hamidi H, Alanko J, Sahgal P, Ivaska J. Integrin traffic – the update. J Cell Sci 2015;128(5):839–52. https://doi.org/10.1242/jcs.161653. URL: http://www.ncbi.nlm.nih.gov/pubmed/25663697, http://www.pubmedcentral.nih.gov/articlerender.fcgi?artid=PMC4342575, http://jcs.biologists.org/cgi/doi/10.1242/jcs.161653.

[68] Stehbens SJ, Paszek M, Pemble H, Ettinger A, Gierke S, Wittmann T. CLASPs link focal-adhesion-associated microtubule capture to localized exocytosis and adhesion site turnover. Nat Cell Biol 2014;16(6):558–70. https://doi.org/10.1038/ncb2975.

[69] Eiseler T, Döppler H, Yan IK, Goodison S, Storz P. Protein kinase D1 regulates matrix metalloproteinase expression and inhibits breast cancer cell invasion. Breast Cancer Res 2009;11(1):R13. https://doi.org/10.1186/bcr2232.

[70] Seetharaman S, Etienne-Manneville S. Microtubules at focal adhesions – a double-edged sword. J Cell Sci 2019;132(19). https://doi.org/10.1242/jcs.232843.

[71] Regen CM, Horwitz AF. Dynamics of beta 1 integrin-mediated adhesive contacts in motile fibroblasts. J Cell Biol 1992;119(5):1347–59. https://doi.org/10.1083/jcb.119.5.1347. URL: https://rupress.org/jcb/article/119/5/1347/14608/Dynamics-of-beta-1-integrinmediated-adhesive.

[72] Palecek SP, Huttenlocher A, Horwitz AF, Lauffenburger DA. Physical and biochemical regulation of integrin release during rear detachment of migrating cells. J Cell Sci 1998;111(Pt 7):929–40. URL: http://www.ncbi.nlm.nih.gov/pubmed/9490637.

[73] Pfaff M, Du X, Ginsberg MH. Calpain cleavage of integrin beta cytoplasmic domains. FEBS Lett 1999;460(1):17–22. https://doi.org/10.1016/s0014-5793(99)01250-8. URL: http://www.ncbi.nlm.nih.gov/pubmed/10571053.

[74] Cuevas BD, Abell AN, Witowsky JA, Yujiri T, Johnson NL, Kesavan K, Ware M, Jones PL, Weed SA, DeBiasi RL, Oka Y, Tyler KL, Johnson GL. MEKK1 regulates calpain-dependent proteolysis of focal adhesion proteins for rear-end detachment of migrating fibroblasts. EMBO J 2003;22(13):3346–55. https://doi.org/10.1093/emboj/cdg322. URL: http://www.ncbi.nlm.nih.gov/pubmed/12839996, http://www.pubmedcentral.nih.gov/articlerender.fcgi?artid=PMC165646.

[75] Chan KT, Bennin DA, Huttenlocher A. Regulation of adhesion dynamics by calpain-mediated proteolysis of focal adhesion kinase (FAK). J Biol Chem 2010;285(15):11418–26. https://doi.org/10.1074/jbc.M109.090746. URL: http://www.ncbi.nlm.nih.gov/pubmed/20150423, http://www.pubmedcentral.nih.gov/articlerender.fcgi?artid=PMC2857020.

[76] Semmrich M, Smith A, Feterowski C, Beer S, Engelhardt B, Busch DH, Bartsch B, Laschinger M, Hogg N, Pfeffer K, Holzmann B. Importance of integrin LFA-1 deactivation for the generation of immune responses. J Exp Med 2005;201(12):1987–98. https://doi.org/10.1084/jem.20041850. URL: http://www.ncbi.nlm.nih.gov/pubmed/15955836, http://www.pubmedcentral.nih.gov/articlerender.fcgi?artid=PMC2212031.

[77] Morin NA, Oakes PW, Hyun Y-M, Lee D, Chin YE, Chin EY, King MR, Springer TA, Shimaoka M, Tang JX, Reichner JS, Kim M. Nonmuscle myosin heavy chain IIA mediates integrin LFA-1 de-adhesion during T lymphocyte migration. J Exp Med 2008;205(1):195–205. https://doi.org/10.1084/jem.20071543. URL: http://www.ncbi.nlm.nih.gov/pubmed/18195072, http://www.pubmedcentral.nih.gov/articlerender.fcgi?artid=PMC2234359.

[78] Pouwels J, Nevo J, Pellinen T, Ylänne J, Ivaska J. Negative regulators of integrin activity. J Cell Sci 2012;125(Pt 14):3271–80. https://doi.org/10.1242/jcs.093641. URL: http://www.ncbi.nlm.nih.gov/pubmed/22822081.

[79] Broussard JA, Webb DJ, Kaverina I. Asymmetric focal adhesion disassembly in motile cells. Curr Opin Cell Biol 2008;20(1):85–90. https://doi.org/10.1016/j.ceb.2007.10.009. URL: http://linkinghub.elsevier.com/retrieve/pii/S0955067407001603.

[80] Smilenov LB, Mikhailov A, Pelham RJ, Marcantonio EE, Gundersen GG. Focal adhesion motility revealed in stationary fibroblasts. Science 1999;286 (5442):1172–4. https://doi.org/10.1126/science.286.5442.1172. URL: http://www.ncbi.nlm.nih.gov/pubmed/10550057.

[81] Ballestrem C, Hinz B, Imhof BA, Wehrle-Haller B. Marching at the front and dragging behind: differential alphaVbeta3-integrin turnover regulates focal adhesion behavior. J Cell Biol 2001;155(7):1319–32. https://doi.org/10.1083/jcb.200107107. URL: http://www.ncbi.nlm.nih.gov/pubmed/11756480, http://www.pubmedcentral.nih.gov/articlerender.fcgi?artid=PMC2199321.

[82] Wehrle-Haller B. Structure and function of focal adhesions. Curr Opin Cell Biol 2012;24(1):116–24. https://doi.org/10.1016/J.CEB.2011.11.001. URL: https://www.sciencedirect.com/science/article/pii/S0955067411001475#bib0090.

[83] Luo B-H, Carman CV, Springer TA. Structural basis of integrin regulation and signaling. Annu Rev Immunol 2007;25:619–47. https://doi.org/10.1146/annurev.immunol.25.022106.141618. URL: http://www.ncbi.nlm.nih.gov/pubmed/17201681, http://www.pubmedcentral.nih.gov/articlerender.fcgi?artid=PMC1952532.

[84] Xiong JP, Stehle T, Diefenbach B, Zhang R, Dunker R, Scott DL, Joachimiak A, Goodman SL, Arnaout MA. Crystal structure of the extracellular segment of integrin alpha Vbeta3. Science (New York, N.Y.) 2001;294(5541):339–45. https://doi.org/10.1126/science.1064535. URL: http://www.ncbi.nlm.nih.gov/pubmed/11546839, http://www.pubmedcentral.nih.gov/articlerender.fcgi?artid=PMC2885948.

[85] Takagi J, Petre BM, Walz T, Springer TA. Global conformational rearrangements in integrin extracellular domains in outside-in and inside-out signaling. Cell 2002;110(5):599–611. URL: http://www.ncbi.nlm.nih.gov/pubmed/12230977.

[86] Mould AP, Barton SJ, Askari JA, Craig SE, Humphries MJ. Role of ADMIDAS Cation-binding Site in Ligand Recognition by Integrin α 5 β 1t. J Biol Chem 2003;278(51):51622–9. https://doi.org/10.1074/jbc.M306655200. URL: http://www.ncbi.nlm.nih.gov/pubmed/14532288.

[87] Chen J, Salas A, Springer TA. Bistable regulation of integrin adhesiveness by a bipolar metal ion cluster. Nat Struct Biol 2003;10(12):995–1001. https://doi.org/10.1038/nsb1011. URL: http://www.ncbi.nlm.nih.gov/pubmed/14608374.

[88] Tadokoro S, Shattil SJ, Eto K, Tai V, Liddington RC, de Pereda JM, Ginsberg MH, Calderwood DA. No Title 302(5642). https://doi.org/10.1126/science.1086652. URL: http://www.ncbi.nlm.nih.gov/pubmed/14526080.

[89] Shattil SJ, Kim C, Ginsberg MH. The final steps of integrin activation: the end game. Nat Rev Mol Cell Biol 2010;11(4):288–300. https://doi.org/10.1038/nrm2871. URL: http://www.nature.com/doifinder/10.1038/nrm2871.

[90] Harburger DS, Calderwood DA. Integrin signalling at a glance. J Cell Sci 2009;122(Pt 2):159–63. https://doi.org/10.1242/jcs.018093. URL: http://www.ncbi.nlm.nih.gov/pubmed/11739647, http://www.ncbi.nlm.nih.gov/pubmed/19118207, http://www.pubmedcentral.nih.gov/articlerender.fcgi?artid=PMC2714413.

[91] Qin J, Vinogradova O, Plow EF. Integrin bidirectional signaling: a molecular view. PLoS Biol 2004;2(6): . https://doi.org/10.1371/journal.pbio.0020169 e169.

[92] Nishida N, Xie C, Shimaoka M, Cheng Y, Walz T, Springer TA. Activation of leukocyte $\beta 2$ Integrins by conversion from bent to extended conformations. Immunity 2006;25(4):583–94. https://doi.org/10.1016/j.immuni.2006.07.016. URL: http://www.ncbi.nlm.nih.gov/pubmed/17045822, http://linkinghub.elsevier.com/retrieve/pii/S1074761306004274.

[93] Chen X, Xie C, Nishida N, Li Z, Walz T, Springer TA. Requirement of open headpiece conformation for activation of leukocyte integrin alphaXbeta2. Proc Natl Acad Sci USA 2010;107(33):14727–32. https://doi.org/10.1073/pnas.1008663107. URL: http://www.ncbi.nlm.nih.gov/pubmed/20679211, http://www.pubmedcentral.nih.gov/articlerender.fcgi?artid=PMC2930457.

[94] Jin M, Andricioaei I, Springer TA. Conversion between three conformational states of integrin I domains with a C-terminal pull spring studied with molecular dynamics. Structure 2004;12(12):2137–47. https://doi.org/10.1016/j.str.2004.10.005. URL: http://www.ncbi.nlm.nih.gov/pubmed/15576028, http://linkinghub.elsevier.com/retrieve/pii/S0969212604003739.

[95] Puklin-Faucher E, Gao M, Schulten K, Vogel V. How the headpiece hinge angle is opened: new insights into the dynamics of integrin activation. J Cell Biol 2006;175(2):349–60. https://doi.org/10.1083/jcb.200602071. URL: http://www.ncbi.nlm.nih.gov/pubmed/17060501, http://www.pubmedcentral.nih.gov/articlerender.fcgi?artid=PMC2064575.

[96] Lollo BA, Chan KW, Hanson EM, Moy VT, Brian AA. Direct evidence for two affinity states for lymphocyte function-associated antigen 1 on activated T cells. J Biol Chem 1993;268(29):21693–700. URL: http://www.ncbi.nlm.nih.gov/pubmed/8104943.

[97] Shimaoka M, Lu C, Palframan RT, von Andrian UH, McCormack A, Takagi J, et al. Reversibly locking a protein fold in an active conformation with a disulfide bond: integrin alphaL I domains with high affinity and antagonist activity in vivo. Proc Natl Acad Sci USA 2001;98(11):6009–14. https://doi.org/10.1073/pnas.101130498. URL: http://www.ncbi.nlm.nih.gov/pubmed/11353828, http://www.pubmedcentral.nih.gov/articlerender.fcgi?artid=PMC33413.

[98] Constantin G, Majeed M, Giagulli C, Piccio L, Kim JY, Butcher EC, Laudanna C. Chemokines trigger immediate beta2 integrin affinity and mobility changes: differential regulation and roles in lymphocyte arrest under flow. Immunity 2000;13(6):759–69. URL: http://www.ncbi.nlm.nih.gov/pubmed/11163192.

[99] Chan JR, Hyduk SJ, Cybulsky MI. Detecting rapid and transient upregulation of leukocyte integrin affinity induced by chemokines and chemoattractants. J Immunol Methods 2003;273(1–2):43–52. URL: http://www.ncbi.nlm.nih.gov/pubmed/12535796.

[100] Li J, Su Y, Xia W, Qin Y, Humphries MJ, Vestweber D, Cabañas C, Lu C, Springer TA. Conformational equilibria and intrinsic affinities define integrin activation. EMBO J 2017;36(5):629–45. https://doi.org/10.15252/embj.201695803.

[101] Kong F, Li Z, Parks WM, Dumbauld DW, García AJ, Mould AP, Humphries MJ, Zhu C. Cyclic mechanical reinforcement of integrin ligand interactions. Mol Cell 2013;49(6):1060–8. https://doi.org/10.1016/j.molcel.2013.01.015. URL: http://www.ncbi.nlm.nih.gov/pubmed/23416109.

[102] Li Z, Kong F, Zhu C. A model for cyclic mechanical reinforcement. Scientific Rep 2016;6(1):35954. https://doi.org/10.1038/srep35954.

[103] Ye F, Petrich B, Anekal P, Lefort C, Kasirer-Friede A, Shattil S, Ruppert R, Moser M, Fässler R, Ginsberg M. The mechanism of kindlin-mediated activation of integrin $\alpha IIb\beta 3$. Curr Biol 2013;23(22):2288–95. https://doi.org/10.1016/j.cub.2013.09.050. URL: http://www.ncbi.nlm.nih.gov/pubmed/24210614, http://www.pubmedcentral.nih.gov/articlerender.fcgi?artid=PMC3912999 https://linkinghub.elsevier.com/retrieve/pii/S0960982213011974.

[104] Li J, Springer TA. Integrin extension enables ultrasensitive regulation by cytoskeletal force. Proc Natl Acad Sci 2017;114(18):4685–90. https://doi.org/10.1073/pnas.1704171114.

[105] Li J, Springer TA. Energy landscape differences among integrins establish the framework for understanding activation. J Cell Biol 2018;217(1):397–412. https://doi.org/10.1083/jcb.201701169. URL: http://www.ncbi.nlm.nih.gov/pubmed/29122968, http://www.pubmedcentral.nih.gov/articlerender.fcgi?artid=PMC5748972.

[106] Alon R, Kassner PD, Carr MW, Finger EB, Hemler ME, Springer TA. The integrin VLA-4 supports tethering and rolling in flow on VCAM-1. J Cell Biol 1995;128 (6):1243–53. https://doi.org/10.1083/jcb.128.6.1243. URL: http://www.ncbi.nlm.nih.gov/pubmed/7534768, http://www.pubmedcentral.nih.gov/articlerender.fcgi?artid=PMC2120426.

[107] Footer MJ, Kerssemakers JWJ, Theriot JA, Dogterom M. Direct measurement of force generation by actin filament polymerization using an optical trap. Proc Natl Acad Sci USA 2007;104(7):2181–6. https://doi.org/10.1073/pnas.0607052104. URL: http://www.ncbi.nlm.nih.gov/pubmed/17277076, http://www.pubmedcentral.nih.gov/articlerender.fcgi?artid=PMC1892916.

[108] Kovar DR, Pollard TD. Insertional assembly of actin filament barbed ends in association with formins produces piconewton forces. Proc Natl Acad Sci USA 2004;101(41):14725–30. https://doi.org/10.1073/pnas.0405902101. URL: http://www.ncbi.nlm.nih.gov/pubmed/15377785, http://www.pubmedcentral.nih.gov/articlerender.fcgi?artid=PMC522035.

[109] Laudanna C, Kim JY, Constantin G, Butcher EC. Rapid leukocyte integrin activation by chemokines. Immunol Rev 2002;186(1):37–46. https://doi.org/10.1034/j.1600-065X.2002.18604.x.

[110] Chang AC, Mekhdjian AH, Morimatsu M, Denisin AK, Pruitt BL, Dunn AR. Single molecule force measurements in living cells reveal a minimally tensioned integrin state. ACS Nano 2016;10(12):10745–52. https://doi.org/10.1021/acsnano.6b03314.

[111] Sun Z, Costell M, Fässler R. Integrin activation by talin, kindlin and mechanical forces. Nat Cell Biol 2019;21(1):25–31. https://doi.org/10.1038/s41556-018-0234-9.

[112] Kechagia JZ, Ivaska J, Roca-Cusachs P. Integrins as biomechanical sensors of the microenvironment; 2019. https://doi.org/10.1038/s41580-019-0134-2. URL: http://www.nature.com/articles/s41580-019-0134-2.

[113] Bell GI. Models for the specific adhesion of cells to cells; 1978. arXiv:1011.1669v3. https://doi.org/10.1126/science.347575. URL: http://www.ncbi.nlm.nih.gov/pubmed/347575.

[114] Evans E, Ritchie K. Dynamic strength of molecular adhesion bonds. Biophys J 1997;72(4):1541–55. https://doi.org/10.1016/S0006-3495(97)78802-7. URL: http://www.ncbi.nlm.nih.gov/pubmed/9083660, http://www.pubmedcentral.nih.gov/articlerender.fcgi?artid=PMC1184350.

[115] Evans EA, Calderwood DA. Forces and bond dynamics in cell adhesion. Science 316(5828). URL: http://science.sciencemag.org/content/316/5828/1148..

[116] Evans E, Leung A, Hammer D, Simon S. Chemically distinct transition states govern rapid dissociation of single L-selectin bonds under force. Proc Natl Acad Sci USA 2001;98(7):3784–9. https://doi.org/10.1073/pnas.061324998. URL: http://www.ncbi.nlm.nih.gov/pubmed/11274395, http://www.pubmedcentral.nih.gov/articlerender.fcgi?artid=PMC31130.

[117] Evans E, Leung A, Heinrich V, Zhu C. Mechanical switching and coupling between two dissociation pathways in a P-selectin adhesion bond. Proc Natl Acad Sci USA 2004;101(31):11281–6. https://doi.org/10.1073/pnas.0401870101. URL: http://www.ncbi.nlm.nih.gov/pubmed/15277675, http://www.pubmedcentral.nih.gov/articlerender.fcgi?artid=PMC509195.

[118] Yuan C, Chen A, Kolb P, Moy VT. Energy landscape of streptavidin-biotin complexes measured by atomic force microscopy. Biochemistry 2000;39 (33):10219–23. https://doi.org/10.1021/bi992715o.

[119] Pereverzev YV, Prezhdo OV, Forero M, Sokurenko EV, Thomas WE. The two-pathway model for the catch-slip transition in biological adhesion. Biophys J 2005;89(3):1446–54. https://doi.org/10.1529/biophysj.105.062158. URL: http://www.ncbi.nlm.nih.gov/pubmed/15951391, http://www.pubmedcentral.nih.gov/articlerender.fcgi?artid=PMC1366651.

[120] Dembo M, Torney DC, Saxman K, Hammer D. The reaction-limited kinetics of membrane-to-surface adhesion and detachment; 1988.https://doi.org/10.1098/rspb.1988.0038..

[121] Rakshit S, Zhang Y, Manibog K, Shafraz O, Sivasankar S, et al. Ideal, catch, and slip bonds in cadherin adhesion. Proc Natl Acad Sci USA 2012;109(46):18815–20. https://doi.org/10.1073/pnas.1208349109. URL: http://www.ncbi.nlm.nih.gov/pubmed/23112161, http://www.pubmedcentral.nih.gov/articlerender.fcgi?artid=PMC3503169.

[122] Li F, Redick SD, Erickson HP, Moy VT. Force measurements of the alpha5beta1 integrin-fibronectin interaction. Biophys J 2003;84(2 Pt 1):1252–62. https://doi.org/10.1016/S0006-3495(03)74940-6. URL: http://www.ncbi.nlm.nih.gov/pubmed/12547805, http://www.pubmedcentral.nih.gov/articlerender.fcgi?artid=PMC1302701.

[123] Zhang X, Wojcikiewicz E, Moy VT. Force spectroscopy of the leukocyte function-associated antigen-1/intercellular adhesion molecule-1 interaction. Biophys J 2002;83(4):2270–9. https://doi.org/10.1016/S0006-3495(02)73987-8. URL: http://www.ncbi.nlm.nih.gov/pubmed/12324444, http://www.pubmedcentral.nih.gov/articlerender.fcgi?artid=PMC1302315.

[124] Zhang X, Craig SE, Kirby H, Humphries MJ, Moy VT. Molecular basis for the dynamic strength of the integrin $\alpha4\beta1$/VCAM-1 interaction. Biophys J 2004;87(5):3470–8. https://doi.org/10.1529/biophysj.104.045690. URL: http://www.ncbi.nlm.nih.gov/pubmed/15347595, http://www.pubmedcentral.nih.gov/articlerender.fcgi?artid=PMC1304813, https://linkinghub.elsevier.com/retrieve/pii/S0006349504738126.

[125] Kong F, García AJ, Mould AP, Humphries MJ, Zhu C. Demonstration of catch bonds between an integrin and its ligand. J Cell Biol 2009;185(7):1275–84. https://doi.org/10.1083/jcb.200810002. URL: http://www.ncbi.nlm.nih.gov/pubmed/19564406, http://www.pubmedcentral.nih.gov/articlerender.fcgi?artid=PMC2712956, http://jcb.rupress.org/content/185/7/1275.

[126] Pereverzev YV, Prezhdo OV, Sokurenko EV. Allosteric role of the large-scale domain opening in biological catch-binding. Phys Rev E 2009;79(5): . https://doi.org/10.1103/PhysRevE.79.051913. URL: http://www.ncbi.nlm.nih.gov/pubmed/19518486051913.

[127] Pereverzev YV, Prezhdo E, Sokurenko EV. The two-pathway model of the biological catch-bond as a limit of the allosteric model. Biophys J 2011;101(8):2026–36. https://doi.org/10.1016/j.bpj.2011.09.005. URL: http://www.ncbi.nlm.nih.gov/pubmed/22004757 http://www.pubmedcentral.nih.gov/articlerender.fcgi?artid=PMC3192973.

[128] Li Y, Bhimalapuram P, Dinner AR. Model for how retrograde actin flow regulates adhesion traction stresses. J Phys Condens Matter 2010;22(19): . https://doi.org/10.1088/0953-8984/22/19/194113. URL: http://www.ncbi.nlm.nih.gov/pubmed/21386439, http://stacks.iop.org/0953-8984/22/i=19/a=194113?key=crossref.aa16935a0d3792134af7febc6bd6b279194113.

[129] Novikova EA, Storm C. Contractile fibers and catch-bond clusters: a biological force sensor? Biophys J 2013;105(6):1336–45. https://doi.org/10.1016/j.bpj.2013.07.039. URL: http://www.ncbi.nlm.nih.gov/pubmed/24047984, http://www.pubmedcentral.nih.gov/articlerender.fcgi?artid=PMC3785868.

[130] Bangasser BL, Rosenfeld SS, Odde DJ. Determinants of maximal force transmission in a motor-clutch model of cell traction in a compliant microenvironment. Biophys J 2013;105(3):581–92. https://doi.org/10.1016/j.bpj.2013.06.027. URL: http://www.ncbi.nlm.nih.gov/pubmed/23931306, http://www.pubmedcentral.nih.gov/articlerender.fcgi?artid=PMC3736748.

[131] Oakes PW, Bidone TC, Beckham Y, Skeeters AV, Ramirez-San Juan GR, Winter SP, Voth GA, Gardel ML, et al. Lamellipodium is a myosin-independent mechanosensor. Proc Natl Acad Sci 2018;115(11):201715869. https://doi.org/10.1073/pnas.1715869115.

[132] MacKay L, Khadra A. Dynamics of mechanosensitive nascent adhesion formation. Biophys J 2019;117(6):1057–73. https://doi.org/10.1016/j.bpj.2019.08.004. URL: https://www.cell.com/biophysj/fulltext/S0006-3495(19)30671-X.

[133] Rakshit S, Sivasankar S. Biomechanics of cell adhesion: how force regulates the lifetime of adhesive bonds at the single molecule level. Phys Chem Chem Phys 2014;16(6):2211. https://doi.org/10.1039/c3cp53963f. URL: http://xlink.rsc.org/?DOI=c3cp53963f.

[134] Chen W, Lou J, Zhu C. Forcing switch from short- to intermediate- and long-lived states of the alphaA domain generates LFA-1/ICAM-1 catch bonds. J Biol Chem 2010;285(46):35967–78. https://doi.org/10.1074/jbc.M110.155770. URL: http://www.ncbi.nlm.nih.gov/pubmed/20819952, http://www.pubmedcentral.nih.gov/articlerender.fcgi?artid=PMC2975219.

[135] Chen Y, Lee H, Tong H, Schwartz M, Zhu C. Force regulated conformational change of integrin $\alpha V\beta3$. Matrix Biol. 2017;60–61:70–85. https://doi.org/10.1016/j.matbio.2016.07.002. URL: http://www.ncbi.nlm.nih.gov/pubmed/27423389, http://www.pubmedcentral.nih.gov/articlerender.fcgi?artid=PMC5237428.

[136] Rosetti F, Chen Y, Sen M, Thayer E, Azcutia V, Herter J, Luscinskas F, Cullere X, Zhu C, Mayadas T. A lupus-associated Mac-1 variant has defects in integrin allostery and interaction with ligands under force. Cell Rep 2015;10(10):1655–64. https://doi.org/10.1016/J.CELREP.2015.02.037.

[137] Hu J, Lipowsky R, Weikl TR. Binding constants of membrane-anchored receptors and ligands depend strongly on the nanoscale roughness of membranes. Proc Natl Acad Sci USA 2013;110(38):15283–8. https://doi.org/10.1073/pnas.1305766110. URL: http://www.ncbi.nlm.nih.gov/pubmed/24006364, http://www.pubmedcentral.nih.gov/articlerender.fcgi?artid=PMC3780905.

[138] Xu G-K, Hu J, Lipowsky R, Weikl TR. Binding constants of membrane-anchored receptors and ligands: a general theory corroborated by Monte Carlo simulations. J Chem Phys 2015;143(24): . https://doi.org/10.1063/1.4936134243136.

[139] Xu G-K, Qian J, Hu J. The glycocalyx promotes cooperative binding and clustering of adhesion receptors. Soft Matter 2016;12(20):4572–83. https://doi.org/10.1039/C5SM03139G.

[140] Doyle A, Marganski W, Lee J, Goeckeler Z, Côté G, Wysolmerski R. Calcium transients induce spatially coordinated increases in traction force during the movement of fish keratocytes. J Cell Sci 2004;117(Pt 11):2203–14. https://doi.org/10.1242/jcs.01087. URL: http://www.ncbi.nlm.nih.gov/pubmed/10639334, http://www.ncbi.nlm.nih.gov/pubmed/15126622.

[141] Jannat R, Dembo M, Hammer D. Traction forces of neutrophils migrating on compliant substrates. Biophys J 2011;101(3):575–84. https://doi.org/10.1016/J.BPJ.2011.05.040. URL: https://www.sciencedirect.com/science/article/pii/S0006349511006102.

[142] Alberts B, Johnson A, Lewis J, Raff M, Roberts K, Walter P. Molecular biology of the cell. New York: Garland Science; 2002.

[143] King MR. Principles of cellular engineering: understanding the biomolecular interface. Elsevier Academic Press; 2006. URL: https://www.sciencedirect.com/book/9780123693921/principles-of-cellular-engineering.

[144] Paszek MJ, DuFort CC, Rossier O, Bainer R, Mouw JK, Godula K, Hudak JE, Lakins JN, Wijekoon AC, Cassereau L, Rubashkin MG, Magbanua MJ, Thorn KS, Davidson MW, Rugo HS, Park JW, Hammer DA, Giannone G, Bertozzi CR, Weaver VM, et al. The cancer glycocalyx mechanically primes integrin-mediated growth and survival. Nature 2014;511(7509):319–25. https://doi.org/10.1038/nature13535. URL: http://www.ncbi.nlm.nih.gov/pubmed/25030168, http://www.pubmedcentral.nih.gov/articlerender.fcgi?artid=PMC4487551.

[145] Paszek MJ, Boettiger D, Weaver VM, Hammer DA. Integrin clustering is driven by mechanical resistance from the glycocalyx and the substrate. PLoS Comput Biol 2009;5(12): . https://doi.org/10.1371/journal.pcbi.1000604e1000604.

[146] Hu J, Xu G-K, Lipowsky R, Weikl TR. Binding kinetics of membrane-anchored receptors and ligands: molecular dynamics simulations and theory. J Chem Phys 2015;143(24): . https://doi.org/10.1063/1.4936135243137.

[147] Changede R, Cai H, Wind S, Sheetz MP. Ligand geometry controls adhesion formation via integrin clustering. bioRxiv 2018;435826. https://doi.org/10.1101/435826. URL: https://www.biorxiv.org/content/10.1101/435826v1.

[148] Schwarz US, Erdmann T, Bischofs IB. Focal adhesions as mechanosensors: the two-spring model. BioSystems 2006;83(2–3):225–32. https://doi.org/10.1016/j.biosystems.2005.05.019. arXiv:0608006. URL: https://www.sciencedirect.com/science/article/pii/S0303264705001310.

[149] Erdmann T, Schwarz US. Stability of adhesion clusters under constant force. Phys Rev Lett 2004;92(10):108102. https://doi.org/10.1103/PhysRevLett.92.108102. arXiv:0401533.

[150] Schwarz US, Safran SA. Physics of adherent cells. Rev Modern Phys 2013;85(3):1327–81. https://doi.org/10.1103/RevModPhys. 85.1327.

[151] van Kampen NG. Stochastic processes in physics and chemistry. 3rd ed. North Holland; 2007.

[152] Changede R, Xu X, Margadant F, Sheetz MP, Critchley D, Ravasio A, Chen Z, Wang Y, Kawauchi I, Al E. Nascent integrin adhesions form on all matrix rigidities after integrin activation. Develop Cell 2015;35(5):614–21. https://doi.org/10.1016/j.devcel.2015.11.001. URL: http://www.ncbi.nlm.nih.gov/pubmed/26625956, http://linkinghub.elsevier.com/retrieve/pii/S1534580715007157.

[153] Roca-Cusachs P, Gauthier NC, Del Rio A, Sheetz MP. Clustering of alpha(5)beta(1) integrins determines adhesion strength whereas alpha(v)beta(3) and talin enable mechanotransduction. Proc Natl Acad Sci USA 2009;106(38):16245–50. https://doi.org/10.1073/pnas.0902818106. URL: http://www.ncbi.nlm.nih.gov/pubmed/19805288, http://www.pubmedcentral.nih.gov/articlerender.fcgi?artid=PMC2752568.

[154] Balcioglu HE, van Hoorn H, Donato DM, Schmidt T, Danen EH. The integrin expression profile modulates orientation and dynamics of force transmission at cell-matrix adhesions. J Cell Sci 2015;128(7):1316–26. https://doi.org/10.1242/jcs.156950. URL: http://www.ncbi.nlm.nih.gov/pubmed/11973360, http://www.ncbi.nlm.nih.gov/pubmed/25663698.

[155] Novikova EA, Storm C. Evolving roles and dynamics for catch and slip bonds during adhesion cluster maturation. arXiv:1908.08934. URL: http://arxiv.org/abs/1908.08934.

[156] Chiu CL, Aguilar JS, Tsai CY, Wu GK, Gratton E, Digman MA. Nanoimaging of focal adhesion dynamics in 3D. PLoS ONE 2014;9(6): . https://doi.org/10.1371/journal.pone.0099896. URL: http://www.ncbi.nlm.nih.gov/pubmed/24959851,http://www.pubmedcentral.nih.gov/articlerender.fcgi?artid=PMC4069057e99896.

[157] Hoffmann J-E, Fermin Y, Stricker RL, Ickstadt K, Zamir E. Symmetric exchange of multi-protein building blocks between stationary focal adhesions and the cytosol. eLife 3.https://doi.org/10.7554/eLife.02257..

[158] Choi CK, Zareno J, Digman MA, Gratton E, Horwitz AR. Cross-correlated fluctuation analysis reveals phosphorylation-regulated paxillin-fak complexes in nascent adhesions. Biophys J 2011;100(3):583–92. https://

doi.org/10.1016/j.bpj.2010.12.3719. URL: https://www.sciencedirect.com/science/article/pii/S0006349510052926.

[159] Falkenberg CV, Blinov ML, Loew LM. Pleomorphic ensembles: formation of large clusters composed of weakly interacting multivalent molecules. Biophys J 2013;105(11):2451–60. https://doi.org/10.1016/j.bpj.2013.10.016. URL: http://www.ncbi.nlm.nih.gov/pubmed/24314076, http://www.pubmedcentral.nih.gov/articlerender.fcgi?artid=PMC3853317, https://linkinghub.elsevier.com/retrieve/pii/S0006349513011478.

[160] Webb DJ, Donais K, Whitmore LA, Thomas SM, Turner CE, Parsons JT, Horwitz AF, et al. FAK-Src signalling through paxillin, ERK and MLCK regulates adhesion disassembly. Nat Cell Biol 2004;6(2):154–61. https://doi.org/10.1038/ncb1094. URL: http://www.ncbi.nlm.nih.gov/pubmed/14743221.

[161] Wolfenson H, Bershadsky A, Henis YI, Geiger B. Actomyosin-generated tension controls the molecular kinetics of focal adhesions. J Cell Sci 2011;124(Pt 9):1425–32. https://doi.org/10.1242/jcs.077388. URL: http://www.ncbi.nlm.nih.gov/pubmed/21486952, http://www.pubmedcentral.nih.gov/articlerender.fcgi?artid=PMC3078811.

[162] Stehbens SJ, Wittmann T. Analysis of focal adhesion turnover. A quantitative live-cell imaging example. In: Methods in Cell Biology. vol. 123. NIH Public Access; 2014. pp. 335–346.https://doi.org/10.1016/B978-0-12-420138-5.00018-5. URL: http://www.ncbi.nlm.nih.gov/pubmed/24974036, http://www.pubmedcentral.nih.gov/articlerender.fcgi?artid=PMC4198331.

[163] Rajah A, Boudreau CG, Ilie A, Wee T-L, Tang K, Borisov AZ, Orlowski J, Brown CM. Paxillin S273 phosphorylation regulates adhesion dynamics and cell migration through a common protein complex with PAK1 and βPIX. Scientific Rep 2019;9(1):11430. https://doi.org/10.1038/s41598-019-47722-3. URL: http://www.nature.com/articles/s41598-019-47722-3.

[164] Gov NS. Modeling the size distribution of focal adhesions. Biophys J 2006;91(8):2844–7. https://doi.org/10.1529/biophysj.106.088484. URL: http://www.ncbi.nlm.nih.gov/pubmed/16861281, http://www.pubmedcentral.nih.gov/articlerender.fcgi?artid=PMC1578473.

[165] Swaminathan V, Fischer RS, Waterman CM. The FAK-Arp2/3 interaction promotes leading edge advance and haptosensing by coupling nascent adhesions to lamellipodia actin. Mol Biol Cell 2016;27(7):1085–100. https://doi.org/10.1091/mbc.E15-08-0590. URL: http://www.molbiolcell.org/cgi/doi/10.1091/mbc.E15-08-0590.

[166] Hansen SD, Mullins RD. VASP, is a processive actin polymerase that requires monomeric actin for barbed end association. J Cell Biol 191(3), 2010;:571–84. https://doi.org/10.1083/jcb.201003014. URL: http://www.ncbi.nlm.nih.gov/pubmed/21041447, http://www.pubmedcentral.nih.gov/articlerender.fcgi?artid=PMC3003327.

[167] Nicolas A, Safran SA. Elastic deformations of grafted layers with surface stress. Phys Rev E 2004;69(5): . https://doi.org/10.1103/PhysRevE.69.051902051902.

[168] Besser A, Schwarz US. Coupling biochemistry and mechanics in cell adhesion: a model for inhomogeneous stress fiber contraction. New J Phys 2007;9(11). https://doi.org/10.1088/1367-2630/9/11/425. pp. 425–425. arXiv:0707.2551. URL: http://stacks.iop.org/1367-2630/9/i=11/a=425?key=crossref.ecbea7e76b72769c1d0b28e0c4ab3e38.

[169] Bruinsma R. Theory of force regulation by nascent adhesion sites. Biophys J 2005;89(1):87. https://doi.org/10.1529/BIOPHYSJ.104.048280. URL: http://www.ncbi.nlm.nih.gov/pubmed/15849245, http://www.pubmedcentral.nih.gov/articlerender.fcgi?artid=PMC1366582.

[170] Diamant H, Andelman D. Kinetics of surfactant adsorption at fluid-fluid interfaces. J Phys Chem 1996;100(32):13732–42. https://doi.org/10.1021/jp960377k.

[171] Han SJ, Bielawski KS, Ting LH, Rodriguez ML, Sniadecki NJ. Decoupling substrate stiffness, spread area, and micropost density: a close spatial relationship between traction forces and focal adhesions. Biophys J 2012;103(4):640–8. https://doi.org/10.1016/j.bpj.2012.07.023. URL: http://www.pubmedcentral.nih.gov/articlerender.fcgi?artid=3443781&tool=pmcentrez&rendertype=abstract.

[172] Peyton SR, Putnam AJ. Extracellular matrix rigidity governs smooth muscle cell motility in a biphasic fashion. J Cell Physiol 2005;204(1):198–209. https://doi.org/10.1002/jcp.20274.

[173] Cao X, Ban E, Baker BM, Lin Y, Burdick JA, Chen CS, et al. Multiscale model predicts increasing focal adhesion size with decreasing stiffness in fibrous matrices. Proc Natl Acad Sci USA 2017;114(23):E4549–55. https://doi.org/10.1073/pnas.1620486114. URL: http://www.ncbi.nlm.nih.gov/pubmed/28468803, http://www.pubmedcentral.nih.gov/articlerender.fcgi?artid=PMC5468675.

[174] Shemesh T, Geiger B, Bershadsky AD, Kozlov MM. Focal adhesions as mechanosensors: a physical mechanism. Proc Natl Acad Sci 2005;102(35):12383–8. https://doi.org/10.1073/PNAS.0500254102. URL: https://www.pnas.org/content/102/35/12383.

[175] Olberding JE, Thouless MD, Arruda EM, Garikipati K. The non-equilibrium thermodynamics and kinetics of focal adhesion dynamics. PLoS ONE 2010;5(8): . https://doi.org/10.1371/journal.pone.0012043e12043.

[176] Lombardi ML, Knecht DA, Dembo M, Lee J. Traction force microscopy in Dictyostelium reveals distinct roles for myosin II motor and actin-crosslinking activity in polarized cell movement. J Cell Sci 2007;120(Pt 9):1624–34. https://doi.org/10.1242/jcs.002527. URL: http://www.ncbi.nlm.nih.gov/pubmed/7622597, http://www.ncbi.nlm.nih.gov/pubmed/17452624.

[177] Roux C, Duperray A, Laurent VM, Michel R, Peschetola V, Verdier C, Étienne J. Prediction of traction forces of motile cells. Interface Focus 2016;6(5):20160042. https://doi.org/10.1098/rsfs.2016.0042.

[178] Anderson KI, Cross R. Contact dynamics during keratocyte motility. Curr Biol 2000;10(5):253–60. https://doi.org/10.1016/S0960-9822(00)00357-2. URL: https://www.sciencedirect.com/science/article/pii/S0960982200003572?via%3Dihub.

[179] Messi Z, Bornert A, Raynaud F, Verkhovsky A. Traction forces control cell-edge dynamics and mediate distance-sensitivity during cell polarization. bioRxiv 2019;745687. https://doi.org/10.1101/745687. URL: https://www.biorxiv.org/content/10.1101/745687v1.full.

[180] Hu S, Tee Y-H, Kabla A, Zaidel-Bar R, Bershadsky A, Hersen P. Structured illumination microscopy reveals focal adhesions are composed of linear subunits. Cytoskeleton 2015;72(5):235–45. https://doi.org/10.1002/cm.21223.

[181] Stutchbury B, Atherton P, Tsang R, Wang D-Y, Ballestrem C. Distinct focal adhesion protein modules control different aspects of mechanotransduction. J Cell Sci 2017;130(9):1612–24. https://doi.org/10.1242/jcs.195362. URL: http://www.ncbi.nlm.nih.gov/pubmed/28302906, http://www.pubmedcentral.nih.gov/articlerender.fcgi?artid=PMC5450230.

[182] Xu G-K, Yang C, Du J, Feng X-Q. Integrin activation and internalization mediated by extracellular matrix elasticity: a biomechanical model. J Biomech 2014;47(6):1479–84. https://doi.org/10.1016/J.JBIOMECH.2014.01.023. URL: https://www.sciencedirect.com/science/article/pii/S0021929014000530?via%3Dihub.

[183] Kaelble DH. Theory and analysis of peel adhesion: bond stresses and distributions. Trans Soc Rheol 1960;4(1):45–73. https://doi.org/10.1122/1.548868.

[184] Sens P, Turner MS. Theoretical model for the formation of caveolae and similar membrane invaginations. Biophys J 2004;86(4):2049–57. https://doi.org/10.1016/S0006-3495(04)74266-6. URL: http://www.ncbi.nlm.nih.gov/pubmed/15041647, http://www.pubmedcentral.nih.gov/articlerender.fcgi?artid=PMC1304058.

[185] Du J, Chen X, Liang X, Zhang G, Xu J, He L, Zhan Q, Feng X-Q, Chien S, Yang C, et al. Integrin activation and internalization on soft ECM as a mechanism of induction of stem cell differentiation by ECM elasticity. Proc Natl Acad Sci USA 2011;108(23):9466–71. https://doi.org/10.1073/pnas.1106467108. URL: http://www.ncbi.nlm.nih.gov/pubmed/21593411, http://www.pubmedcentral.nih.gov/articlerender.fcgi?artid=PMC3111285.

[186] Erdmann T, Schwarz US. Stochastic dynamics of adhesion clusters under shared constant force and with rebinding. J Chem Phys 2004;121(18):8997–9017. https://doi.org/10.1063/1.1805496. arXiv:0405247. URL: http://www.ncbi.nlm.nih.gov/pubmed/15527366.

[187] Walcott S, Kim D-H, Wirtz D, Sun SX. Nucleation and decay initiation are the stiffness-sensitive phases of focal adhesion maturation. Biophys J 2011;101(12):2919–28. https://doi.org/10.1016/j.bpj.2011.11.010. URL: http://www.ncbi.nlm.nih.gov/pubmed/22208190, http://www.pubmedcentral.nih.gov/articlerender.fcgi?artid=PMC3244057.

[188] Malik-Sheriff RS, Imtiaz S, Grecco HE, Zamir E. Diverse patterns of molecular changes in the mechano-responsiveness of focal adhesions. Scientific Rep 2018;8(1):2187. https://doi.org/10.1038/s41598-018-20252-0. URL: http://www.nature.com/articles/s41598-018-20252-0.

[189] Chien F-C, Kuo CW, Yang Z-H, Chueh D-Y, Chen P. Exploring the formation of focal adhesions on patterned surfaces using super-resolution imaging. Small 2011;7(20):2906–13. https://doi.org/10.1002/smll.201100753.

[190] Pontes B, Monzo P, Gole L, Le Roux AL, Kosmalska AJ, Tam ZY, Luo W, Kan S, Viasnoff V, Roca-Cusachs P, Tucker-Kellogg L, Gauthier NC. Membrane tension controls adhesion positioning at the leading edge of cells. J Cell Biol 2017;216(9):2959–77. https://doi.org/10.1083/jcb.201611117. URL: http://www.ncbi.nlm.nih.gov/pubmed/28687667, http://www.pubmedcentral.nih.gov/articlerender.fcgi?artid=PMC5584154.

[191] Schulte C, Ferraris GMS, Oldani A, Galluzzi M, Podestà A, Puricelli L, de Lorenzi V, Lenardi C, Milani P, Sidenius N. Lamellipodial tension, not integrin/ligand binding, is the crucial factor to realise integrin activation and cell migration. Eur J Cell Biol 2016;95(1):1–14. https://doi.org/10.1016/j.ejcb.2015.10.002. URL: http://linkinghub.elsevier.com/retrieve/pii/S0171933515300121.

[192] Jiang G, Giannone G, Critchley DR, Fukumoto E, Sheet MP. Two-piconewton slip bond between fibronectin and the cytoskeleton depends on talin. Nature 2003;424(6946):334–7. https://doi.org/10.1038/nature01805. URL: http://www.ncbi.nlm.nih.gov/pubmed/12867986, http://www.nature.com/articles/nature01805.

[193] Huang DL, Bax NA, Buckley CD, Weis WI, Dunn AR. Vinculin forms a directionally asymmetric catch bond with F-actin. Science 2017;357(6352):703–6. https://doi.org/10.1126/science.aan2556. URL: http://www.ncbi.nlm.nih.gov/pubmed/28818948, http://www.pubmedcentral.nih.gov/articlerender.fcgi?artid=PMC5821505.

[194] Wu Z, Plotnikov SV, Moalim AY, Waterman CM, Liu J. Two distinct actin networks mediate traction oscillations to confer focal adhesion mechanosensing. Biophys J 2017;112(4):780–94. https://doi.org/10.1016/j.bpj.2016.12.035. URL: http://www.ncbi.nlm.nih.gov/pubmed/28256237, http://www.pubmedcentral.nih.gov/articlerender.fcgi?artid=PMC5340160.

[195] Nayal A, Webb DJ, Brown CM, Schaefer EM, Vicente-Manzanares M, Horwitz AR. Paxillin phosphorylation at Ser273 localizes a GIT1-PIX-PAK complex and regulates adhesion and protrusion dynamics. J Cell Biol 2006;173(4):587–9. https://doi.org/10.1083/jcb.200509075. URL: http://www.ncbi.nlm.nih.gov/

pubmed/16717130, http://www.pubmedcentral.nih.gov/articlerender.fcgi?artid=PMC2063867,http://www.pubmedcentral.nih.gov/articlerender.fcgi?artid=2063867&tool=pmcentrez&rendertyp.

[196] Goult BT, Yan J, Schwartz MA. Talin as a mechanosensitive signaling hub. J Cell Biol 2018;217(11):3776–84. https://doi.org/10.1083/jcb.201808061. URL: http://www.ncbi.nlm.nih.gov/pubmed/30254032, http://www.pubmedcentral.nih.gov/articlerender.fcgi?artid=PMC6219721.

[197] Elosegui-Artola A, Oria R, Chen Y, Kosmalska A, Pérez-González C, Castro N, Zhu C, Trepat X, Roca-Cusachs P. Mechanical regulation of a molecular clutch defines force transmission and transduction in response to matrix rigidity. Nat Cell Biol 2016;18(5):540–8. https://doi.org/10.1038/ncb3336. URL: http://www.nature.com/articles/ncb3336.

[198] Roca-Cusachs P, Iskratsch T, Sheetz MP. Finding the weakest link-exploring integrin-mediated mechanical molecular pathways; 2012.https://doi.org/10.1242/jcs.095794. URL: http://www.ncbi.nlm.nih.gov/pubmed/22797926, http://www.pubmedcentral.nih.gov/articlerender.fcgi?artid=PMC6518164.

[199] Burgos-Bravo F, Figueroa NL, Casanova-Morales N, Quest AFG, Wilson CAM, Leyton L. Single-molecule measurements of the effect of force on Thy-1/α vβ3-integrin interaction using nonpurified proteins. Mol Biol Cell 2018;29 (3):326–38. https://doi.org/10.1091/mbc.E17-03-0133. URL: http://www.ncbi.nlm.nih.gov/pubmed/29212879, http://www.pubmedcentral.nih.gov/articlerender.fcgi?artid=PMC5996956.

[200] Hanna S, El-Sibai M. Signaling networks of Rho GTPases in cell motility. Cell Signal 2013;25(10):1955–61. https://doi.org/10.1016/j.cellsig.2013.04.009. URL: http://www.ncbi.nlm.nih.gov/pubmed/23669310, https://linkinghub.elsevier.com/retrieve/pii/S0898656813001241.

[201] Warner H, Wilson BJ, Caswell PT. Control of adhesion and protrusion in cell migration by Rho GTPases. Curr Opin Cell Biol 2019;56:64–70. https://doi.org/10.1016/J.CEB.2018.09.003. URL: https://www.sciencedirect.com/science/article/pii/S095506741830111X.

[202] Lawson CD, Burridge K. The on-off relationship of Rho and Rac during integrin-mediated adhesion and cell migration. Small GTPases 2014;5(1): . https://doi.org/10.4161/sgtp.27958e27958.

[203] Mori Y, Jilkine A, Edelstein-Keshet L. Wave-pinning and cell polarity from a bistable reaction-diffusion system. Biophys J 2008;94(9):3684–97. https://doi.org/10.1529/biophysj.107.120824. URL: http://www.ncbi.nlm.nih.gov/pubmed/18212014, http://www.pubmedcentral.nih.gov/articlerender.fcgi?artid=PMC2292363, http://linkinghub.elsevier.com/retrieve/pii/S0006349508704442.

[204] Dawes AT, Edelstein-Keshet L. Phosphoinositides and Rho proteins spatially regulate actin polymerization to initiate and maintain directed movement in a one-dimensional model of a motile cell. Biophys J 2007;92(3):744–68. https://doi.org/10.1529/biophysj.106.090514. URL: http://www.ncbi.nlm.nih.gov/pubmed/17098793, http://www.pubmedcentral.nih.gov/articlerender.fcgi?artid=PMC1779977, http://linkinghub.elsevier.com/retrieve/pii/S0006349507708858.

[205] Machacek M, Hodgson L, Welch C, Elliott H, Pertz O, Nalbant P, Abell A, Johnson GL, Hahn KM, Danuser G. Coordination of Rho GTPase activities during cell protrusion. Nature 2009;461(7260):99–103. https://doi.org/10.1038/nature08242. URL: http://www.ncbi.nlm.nih.gov/pubmed/19693013, http://www.pubmedcentral.nih.gov/articlerender.fcgi?artid=PMC2885353, http://www.nature.com/articles/nature08242.

[206] Wei C, Wang X, Chen M, Ouyang K, Song L-S, Cheng H. Calcium flickers steer cell migration. Nature 2009;457(7231):901–5. https://doi.org/10.1038/nature07577. URL: http://www.ncbi.nlm.nih.gov/pubmed/19118385, http://www.pubmedcentral.nih.gov/articlerender.fcgi?artid=PMC3505761.

[207] Lieber A, Yehudai-Resheff S, Barnhart E, Theriot J, Keren K. Membrane tension in rapidly moving cells is determined by cytoskeletal forces. Curr Biol 2013;23(15):1409–17. https://doi.org/10.1016/J.CUB.2013.05.063. URL: https://www.sciencedirect.com/science/article/pii/S096098221300688X.

[208] Huttenlocher A, Palecek SP, Lu Q, Zhang W, Mellgren RL, Lauffenburger DA, Ginsberg MH, Horwitz AF. Regulation of cell migration by the calcium-dependent protease calpain. J Biol Chem 1997;272(52):32719–22. https://doi.org/10.1074/jbc.272.52.32719. URL: http://www.ncbi.nlm.nih.gov/pubmed/9407041.

[209] Glading A, Lauffenburger DA, Wells A. Cutting to the chase: calpain proteases in cell motility. Trends Cell Biol 2002;12(1):46–54. https://doi.org/10.1016/s0962-8924(01)02179-1. URL: http://www.ncbi.nlm.nih.gov/pubmed/11854009.

[210] Franco SJ, Huttenlocher A. Regulating cell migration: calpains make the cut. J Cell Sci 2005;118(Pt 17):3829–38. https://doi.org/10.1242/jcs.02562. URL: http://www.ncbi.nlm.nih.gov/pubmed/16129881.

[211] Bhatt A, Kaverina I, Otey C, Huttenlocher A. Regulation of focal complex composition and disassembly by the calcium-dependent protease calpain. J Cell Sci 2002;115(Pt 17):3415–25. URL: http://www.ncbi.nlm.nih.gov/pubmed/12154072.

[212] Alberty RA. Thermodynamics of Biochemical Reactions. Hoboken, NJ, USA: John Wiley & Sons, Inc.; 2003. https://doi.org/10.1002/0471332607.

[213] Sevilla FJ, Olivares-Quiroz L. Chemical potential for the interacting classical gas and the ideal quantum gas obeying a generalized exclusion principle. Eur J Phys 2012;33:709–22. https://doi.org/10.1088/0143-0807/33/3/709.

[214] McNaught AD, Wilkinson A. IUPAC. Compendium of Chemical Terminology (the Gold Book). IUPAC Compendium of Chemical Terminology.https://doi.org/10.1351/goldbook.R05156..

[215] Voit EO, Martens HA, Omholt SW. 150 years of the mass action law. PLoS Comput Biol 2015;11(1): . https://doi.org/10.1371/journal.pcbi.1004012e1004012.

[216] Hänggi P, Talkner P, Borkovec M. Reaction-rate theory: fifty years after Kramers. Rev Modern Phys 1990;62(2):251–341. https://doi.org/10.1103/RevModPhys. 62.251.

[217] van't Hoff JH. Etudes de dynamique chimique. Amsterdam: Frederik Muller; 1884.

[218] Arrhenius S. Über die Reaktionsgeschwindigkeit bei der Inversion von Rohrzucker durch Säuren. Z Phys Chem 4U (1).https://doi.org/10.1515/zpch-1889-0416. URL: http://www.degruyter.com/view/j/zpch.1889.4.issue-1/zpch-1889-0416/zpch-1889-0416.xml.

[219] Bazant MZ. 10.626. Fall 2011. Electrochemical Energy Systems Massachusetts Institute of Technology: MIT OpenCouseWare. URL: http://ocw.mit.edu.

[220] Bazant MZ. Theory of chemical kinetics and charge transfer based on nonequilibrium thermodynamics. Acc Chem Res 2013;46(5):1144–60. https://doi.org/10.1021/ar300145c.

[221] Hill TL, Kirschner MW. Bioenergetics and kinetics of microtubule and actin filament assembly-disassembly. Int Rev Cytol 1982;78(C):1–125. https://doi.org/10.1016/S0074-7696(08)60105-9. URL: https://www.sciencedirect.com/science/article/pii/S0074769608601059.

[222] Kong D, Ji B, Dai L. Stabilizing to disruptive transition of focal adhesion response to mechanical forces. J Biomech 2010;43(13):2524–9. https://doi.org/10.1016/J.JBIOMECH.2010.05.019. URL: https://www.sciencedirect.com/science/article/pii/S0021929010002927.